

Authors' response to comments made by anonymous reviewer #1:

This study examines the role of NH₃ emissions in global aerosol chemical composition and acidity. The study uses the EMAC model with three different emissions scenarios to quantify effects on size-resolved inorganic aerosol composition and pH. The study observes a link between NH₃ emissions and pH, with complex effects that vary regionally. The study is the first, to my knowledge, to examine predictions of aerosol pH and the sensitivity of pH to different emissions scenarios on a global scale. The study highlights some current model limitations that contribute to challenges predicting pH. The manuscript is very well written and nicely organized. The scope is certainly a fit for ACP and I believe it will be of interest to a broad audience once a number of issues are addressed.

We thank the reviewer for the thoughtful and positive comments on our manuscript. We greatly appreciate the constructive feedback provided, which has helped us improve the clarity and overall quality of the manuscript. Below, we provide a point-by-point response (in black) to all the issues raised (in red).

Specific Comments:

1. A significant issue with the manuscript is the predictions of pH in arid regions of the globe. Thermodynamic equilibrium models, including ISORROPIA, are challenged to represent aerosol pH when relative humidity is low (e.g., see the extensive discussion in Pye et al. (2020)). The manuscript contains significant discussion of results in dry, arid regions – e.g., the Middle East, and over desert regions. The physical interpretation of these results is ambiguous unless the predictions of ALWC and aerosol pH in these regions are more closely scrutinized. The associated discussions likely need substantial revision, or at least more discussion about the potential problems of such predictions under low RH conditions.

We thank the reviewer for highlighting the limitations of thermodynamic equilibrium models under low relative humidity (RH) conditions. We fully acknowledge that predicting aerosol pH in arid regions remains a significant challenge, as discussed in Pye et al. (2020). Discrepancies among thermodynamic models tend to grow as RH decreases, primarily due to differences in the assumptions about activity coefficients. For instance, ISORROPIA assumes constant mean activity coefficients and a unity activity coefficient for H⁺, which results in relatively invariant and often lower pH predictions under dry conditions. In contrast, models such as E-AIM incorporate RH-dependent variations in single-ion activity coefficients for both solutes and solvents, potentially leading to more dynamic pH behavior as RH changes. Additionally, the choice between stable and metastable phase state assumptions introduces further uncertainty. Under low RH (e.g., <35%), the metastable assumption allows for supersaturated solutions, enabling pH calculations even at low aerosol liquid water content (ALWC), often resulting in low pH values. Conversely, the stable state permits salt crystallization, and in cases where the aerosol becomes fully solid, pH may no longer be defined. To assess the sensitivity of our results to this assumption, we conducted a simulation using the metastable assumption (Meta case; see Table 1), with results presented in Table 9 and Figure 7. We have revised the relevant discussion sections (especially section 2.2.1) to better reflect these uncertainties and to avoid overinterpreting pH predictions in arid regions.

2. The title and the abstract are misleading because the different emission scenarios vary SO₂ and NO_x emissions at the same time as NH₃. Therefore, interpreting the results is more complex than a typical modeling sensitivity analysis where one factor is varied while all other factors are held constant. In the case of pH, it is not straightforward to attribute the observed changes to the differences in NH₃ because the precursors for aerosol sulfate and nitrate also changed simultaneously. With the emissions in SO₂, NO_x, and NH₃ changing in different directions (some regions, these go up, in other regions, they go down, and not always together), the results were quite complex and not easy to interpret. For example, a conclusion of the study succinctly stated in Line 707 is: “pH changes closely correspond to variations in NH₃ emissions”, however, the study is not really able to derive the quantitative relationship in each region because of the concurrent changes in SO₂ and NO_x. Ultimately, I think the authors need to do more to facilitate interpretation of the results and isolate the effects of individual species on the observed changes in pH, though this is not easy.

We sincerely thank the reviewer for this insightful comment. We acknowledge that the emission scenarios used in our study involve simultaneous changes in SO₂ and NO_x emissions, while NH₃ emissions are not directly varied but are instead represented using three different emission inventories: two bottom-up inventories (CAMS and CEDS_GBD) and one top-down inventory (Luo et al., 2022). This approach allows us to explore the sensitivity of aerosol pH to plausible variations in NH₃ emissions as reflected by different inventory methodologies, rather than through isolated perturbation experiments. We agree that the co-variation of SO₂, NO_x, and NH₃ across these inventories adds complexity to the interpretation of pH changes, and we have revised the manuscript to clearly articulate this point. The title has been revised to “The influence of ammonia emission inventories on the size-resolved global atmospheric aerosol composition and acidity” to more accurately reflect the study. Furthermore, we have expanded the discussion in Section 7 to more explicitly address the interactions among NH₃, SO₂, and NO_x, and we have revised the abstract and conclusion to better reflect the complexity of interpreting pH responses under varying emission inputs and avoid over-attributing pH changes to NH₃ alone.

3. *The authors acknowledge that the size-resolved pH predictions do not follow the expected trend in many cases, as pH does not systematically decrease with decreasing particle diameter for the different size bins in many locations. Only when NH₃ emissions are eliminated does the model predict more acidic smaller particles. The model errors in predictions of NH₃/NH₄⁺ partitioning suggest there are associated errors in the predictions of aerosol pH. Much more discussion of this point is warranted.*

Indeed, our model does not consistently reproduce the expected trend of decreasing pH with decreasing particle size across all regions. This trend is only clearly observed in the no-NH₃ scenario, where smaller particles are predicted to be more acidic than those in the coarse mode. To further investigate this issue, we compared the simulated SNA composition and NH₃/NH₄⁺ partitioning ratios with available observational data. This comparison revealed discrepancies that can contribute to positive biases in pH predictions of submicron particles, particularly an overestimation of NH₃ partitioning into the aerosol phase and an underestimation of acidic components such as sulfate and nitrate, especially over Europe. We have incorporated a more detailed discussion of these findings in Section 6, emphasizing the implications of partitioning errors on size-resolved pH predictions. We highlight the need for caution when interpreting pH trends in regions with high ammonium content in fine aerosol modes, where model uncertainties in gas-particle partitioning can significantly influence the predicted acidity.

4. *A comparison of stable and metastable mode results from thermodynamic models has been done before. However, it has never been done for global simulations, so the present results are quite important because of their scale. I encourage the authors to expand on this discussion and to consider moving Fig. S4 to the main manuscript.*

We thank the reviewer for this valuable suggestion. Karydis et al. (2021) conducted a global-scale comparison of stable and metastable state assumptions and found that the stable-state assumption leads to global average pH values approximately 0.5 units higher than those under metastable conditions. Our study builds on this by providing additional insights into size-resolved pH differences and their regional variability. Our results corroborate the global-scale findings of Karydis et al. (2021) but also reveal that discrepancies between stable and metastable assumptions can be substantially larger, exceeding 2 pH units, in regions with high concentrations of crustal cations and persistently low RH, such as South Asia and the Middle East. Moreover, our analysis highlights how these differences vary across aerosol size modes, offering a more detailed understanding of the thermodynamic behavior of aerosols under varying environmental conditions. In response to the reviewer’s recommendation, we have moved Figure S4 to the main manuscript as Figure 7, and we have expanded the discussion in Section 6 to more thoroughly examine the implications of phase state assumptions for interpreting aerosol acidity, particularly in arid and dust-influenced regions.

5. *Section 2.2.2: it is really not accurate to frame the discussion around H⁺ and H₂O, only. Other particle*

components can affect the aerosol pH by affecting the H^+ activity coefficient. Although ISORROPIA assumes an H^+ activity coefficient of unity, other models that solve for γ_{H^+} would have an effect on pH from other aerosol components.

We agree that it is not fully accurate to frame the discussion of aerosol pH solely in terms of H^+ and H_2O . As correctly noted, other aerosol components, such as sulfate, nitrate, and organics, can significantly influence the ionic strength of the aerosol solution and, consequently, the activity coefficient of H^+ . While ISORROPIA assumes a constant H^+ activity coefficient of unity, this simplification limits its ability to capture composition-dependent effects on pH, particularly under low relative humidity (RH) conditions where ionic strength can vary substantially. In our study, following ISORROPIA's framework, pH is approximated based on free- H^+ molality under the assumption of $\gamma_{H^+} = 1$. Accordingly, our discussion in Section 2.2.2 focuses on variations in free- H^+ concentration as the primary driver of pH changes. We have revised Section 2.2.1 to explicitly acknowledge this limitation and to clarify that our pH estimates do not account for composition-dependent variations in activity coefficients. We also highlight that this simplification may contribute to discrepancies when comparing with models that include a more detailed thermodynamic treatment.

6. *Table 7: why is the SE-USA case from Pye et al. (2020) not included in this comparison? Aerosol pH in this region has been studied extensively and should provide a good point of comparison for the present study.*

We appreciate the reviewer's suggestion to include the SE-USA case from Pye et al. (2020) as a point of comparison. We agree that this region has been extensively studied and offers valuable insights into the aerosol pH behavior. However, the observational period in Pye et al. (2020) (June 6 – July 14, 2013) does not overlap with our simulation period (2009–2012), which limits the direct comparability of the datasets. Nevertheless, we now refer to the findings from that study in section 4.2 to provide additional context and to support the interpretation of our results in the southeastern U.S. region.

7. *For the comparison to the field-derived pH in Xi'an shown in Table 7, the authors are encouraged to consult Guo et al. (2017), who provide a different estimate of aerosol pH in Xi'an. It is not reasonable to request the present manuscript to arbitrate this disagreement, however, the authors should be aware of different pH estimates for this region.*

Similar to our response to Comment 6, the observational period in Guo et al. (2017), which focuses on winter 2013, falls outside our simulation period (2009–2012). Nonetheless, we recognize the importance of acknowledging alternative pH estimates for Xi'an. To reflect this, we have added a reference to Guo et al. (2017) in section 4.2, noting the differences in observational periods and highlighting the variability in reported pH values for this region. While our study does not attempt to reconcile these differences, we agree it is important to be aware of them when interpreting model–observation comparisons.

8. *Overall comment: reconsider the number of sig figs used in many cases. E.g., in Section 5.3 reporting NH_3 emissions to 0.01 Tg and reporting NH_3 lifetimes to the 0.01 day do not likely reflect uncertainties in these values.*

We agree with the reviewer's suggestion regarding numerical precision. We have revised the number of significant figures in Tables 2, 8, and S1, and throughout the related text. Emissions and deposition are now reported to 0.1 Tg yr^{-1} , burdens to 0.1 Tg, and lifetimes to 0.1 days.

9. *Lines 72 – 74: this sentence needs revision – what does “excess NH_3 released to the atmosphere” really mean.*

Due to reductions in SO_2 and NO_x emissions, the atmospheric formation of H_2SO_4 and HNO_3 has declined. Consequently, less NH_3 is required to neutralize these acids. At the same time, NH_3 emissions have remained stable or slightly increased, resulting in a relative surplus of NH_3 in the atmosphere. We have revised the sentence to clarify this point.

155 10. *Color scale of Fig. 1 was quite difficult to determine the magnitude of the changes in many regions.*
We have reconfigured the data intervals and the corresponding color bar to enhance visual clarity and improve the distinction between different regional patterns and gradients.

160 11. *Line 411 and 430 (and elsewhere): best not to use phrases like this...global pH values show that sulfuric acid is rarely fully neutralized. See also Guo et al. (2017).*
We have revised this terminology throughout the manuscript to use more appropriate language.

165 12. *Paragraph lines 549 – 555: I do not follow the discussion in this paragraph.*
We believe that part of the discrepancy in size-resolved pH calculations between models may arise from differences in how particle size distributions and gas-particle partitioning are treated. For example, the EMAC model uses a lognormal size distribution and applies ISORROPIA separately to each size mode to calculate gas-aerosol partitioning. In contrast, other studies (e.g., Kakavas et al., 2021) employ sectional approaches, where gas-aerosol partitioning is first performed on the bulk aerosol phase, and the resulting condensed mass is then distributed across size bins based on the available surface area. These fundamental differences in modeling assumptions can lead to variations in the predicted distribution of aerosol components across size ranges, which in turn affects the calculated size-resolved pH. To clarify this point, we have revised the text to better explain how differences in size distribution and partitioning methods may contribute to the observed discrepancies.

170 13. *Line 562: the effect of NH₃ emissions on SNA formation has been studied for decades. Also, I would not categorize the effect of NH₃ emissions on pH as the “subject of debate,” but rather understudied.*
Thank you for the helpful suggestion. We agree that the role of NH₃ emissions in SNA formation has been extensively studied over the past decades. Additionally, we acknowledge that describing the effect of NH₃ on aerosol pH as a “subject of debate” may be misleading. A more accurate characterization is that this topic remains understudied, particularly in terms of its size-resolved and region-specific impacts in global modeling frameworks. Accordingly, we have revised the sentence in revised manuscript to better reflect the current state of knowledge.

185 14. *Line 704: this is not true in terrestrial regions where highly acidic (e.g., pH < 2) particles are observed or predicted.*
We apologize for the confusion. The original statement was intended to compare high-latitude marine aerosols to those over remote ocean regions, not to terrestrial regions. We have revised the text to clarify that high-latitude marine aerosols are more acidic compared to aerosols over remote oceanic regions.

190 **Technical Corrections:**

1. *Line 67: trend should be plural.*

Thank you for pointing this out. We have corrected the typo.

2. *Line 133: should ‘of’ be added after ‘number’?*

Thank you for the suggestion. We have added “of” after “number” to improve clarity.

195 3. *Table 2 header: ‘cases’ is repeated.*

We have removed the repeated word.

4. *Line 653: do the authors mean ‘marine aerosol’ instead of ‘oceanic’?*

Yes, “marine aerosol” is more accurate in this context. We have revised the text accordingly.

200 **References**

Guo, H., Weber, R. J., and Nenes, A.: High levels of ammonia do not raise fine particle pH sufficiently to

yield nitrogen oxide-dominated sulfate production, *Scientific Reports*, 7, 12109, 10.1038/s41598-017-11704-0, 2017a.

205 Pye, H. O. T., Nenes, A., Alexander, B., Ault, A. P., Barth, M. C., Clegg, S. L., Collett Jr, J. L., Fahey, K. M., Hennigan, C. J., Herrmann, H., Kanakidou, M., Kelly, J. T., Ku, I. T., McNeill, V. F., Riemer, N., Schaefer, T., Shi, G., Tilgner, A., Walker, J. T., Wang, T., Weber, R., Xing, J., Zaveri, R. A., and Zuend, A.: The acidity of atmospheric particles and clouds, *Atmos. Chem. Phys.*, 20, 4809–4888, 10.5194/acp-20-4809-2020, 2020.

210

Authors' response to comments made by anonymous reviewer #2:

Summary

Wang et al. presents a comprehensive investigation of how ammonia (NH₃) emissions affect size-resolved aerosol composition and acidity on a global scale. Using the EMAC atmospheric chemistry-climate model with three different ammonia emission schemes, the authors analyze the complex interactions between ammonium, sulfate and nitrate in different sizes, geographic regions, and chemical environments. Research advances our understanding of atmospheric aerosol dynamics and has significant implications for air quality management and climate modeling. I recommend publication after addressing the following comments.

We thank the reviewer for the thoughtful and positive comments on our manuscript. We appreciate the constructive feedback provided which helped us improve the clarity and quality of the manuscript. Below is a point-by-point response (in black) to all the points raised (in red).

Specific Comments:

1. Research questions and modeling approach lack clarity

The Introduction provides a comprehensive overview of aerosol emission trends and how PM_{2.5} components respond to different clean air policies. It also notes that these responses vary depending on particle size ranges. However, the progress in modeling this size-resolved response is not clearly presented. The intended model for use in this work and its suitability are not well explained, and the scientific question lacks clarity. The authors are encouraged to clearly articulate the rationale for selecting the model, i.e., why EMAC is appropriate for this question?

We thank the reviewer for this valuable feedback. We recognize the importance of clearly articulating both the scientific motivation and the rationale behind our modeling approach. In response, we have thoroughly revised the manuscript to clarify the research objectives and the suitability of the EMAC model for addressing our questions. Specifically, we have updated the final paragraph of the Introduction to clearly state the scientific questions driving this study, including the size-resolved response of aerosol composition and acidity to changes in precursor emissions. Furthermore, we justify the selection of the EMAC model in the introduction and model description (i.e., section 2), emphasizing its state-of-the-art capability to simulate global-scale aerosol–chemistry–climate interactions with size resolution, and its integration with the ISORROPIA-II thermodynamic module for aerosol pH estimation. ISORROPIA-II is a widely used thermodynamic model well-suited for simulating aerosol pH, as it efficiently handles size-resolved inorganic aerosol systems under varying humidity conditions. While it simplifies some aspects (e.g., assuming unity for certain activity coefficients), it has been extensively validated and remains a practical choice for large-scale pH simulations. These revisions aim to provide a more coherent narrative linking the research context, modeling framework, and study objectives.

2. The role of organic aerosols in affecting aerosol pH

Although the main goal of this work is to study the size-resolved SNA and pH response to different ammonium emission inventories, it would be beneficial to include some discussions on the role of organics in influencing these outcomes. As significant components of aerosol particles with diverse hygroscopic properties, organic aerosols can absorb water and impact both aerosol liquid water content and pH. Including a discussion on how organics might alter the size-resolved response would strengthen the analysis.

For example, the reported 104% increase in NH₄⁺ in response to an 18% rise in ammonia emissions could not solely from interactions with sulfate and nitrate, but may partly result from reactions between ammonia and organic acids (e.g., forming ammonium oxalate). These processes can influence pH, especially in the

0–1 μm range. Neglecting the role of organics risks overattributing observed effects to SNA alone.

We appreciate the reviewer's suggestion to further discuss the role of organic aerosols in influencing aerosol pH. While the primary focus of this study is on the size-resolved response of SNA aerosols to changes in ammonia emissions, we agree that organics can also play a role, particularly through their contribution to aerosol liquid water content (ALWC) and, to a lesser extent, their influence on hydrogen ion activity. In our model, the effect of water-soluble organic aerosols on ALWC is accounted for via the GMXe module, which includes both inorganic and organic contributions. Organic aerosol formation is simulated using the ORACLE module, and the associated water uptake is calculated assuming a κ -hygroscopicity value of 0.14 for all organic components (Tsimpidi et al., 2014). This influences the total aerosol water content used in pH calculations. However, our model in the present set-up does not account for chemical interactions between ammonia and organic acids (e.g., formation of ammonium oxalate), and it treats the inorganic and organic aerosol phases independently. Consequently, while organics can indirectly affect pH through water uptake, changes in NH_3 emissions do not influence organic aerosol formation or the associated water content in our simulations. Therefore, the reported increase in NH_4^+ is attributed solely to interactions with inorganic aerosol components. Although the effect of organics on hydrogen ion activity coefficients is not explicitly included, previous studies have shown that water-soluble organic aerosols exert only a minor influence on aerosol pH. For example, Pye et al. (2018) estimated that organic-associated hydrogen ions increase $\text{PM}_{2.5}$ pH by only ~ 0.1 units, while Vasilakos et al. (2018) found that organics induce pH deviations of less than 2% across a range of compounds and environmental conditions. These findings are consistent with other studies (Battaglia Jr et al., 2019; Pye et al., 2020; Guo et al., 2015; Liu et al., 2017), supporting the limited role of organics in modulating aerosol acidity. We have added this clarification to Section 2.2.1, along with a discussion of the model's limitations in representing ammonia–organic interactions.

Minor comments:

1. *Line 170: The cases are not clearly defined in the texts that describe Table 1. What are no NH_3 and Meta cases? You can briefly introduce why you conduct these two cases here. Is Top-Dep case using the Top-down scheme?*

Thank you for pointing this out. In the no NH_3 case, all ammonia emissions are turned off. The Meta case is identical to the base case, except that the ISORROPIA model is run in metastable mode. The Top-Dep case applies the top-down emission scheme. We have added a brief explanation of these simulation cases in lines 176–180 to clarify their purpose and setup.

2. *Line 207: The symbols and Italic fonts used in the texts and equations throughout the paper, such as $E_{\text{NH}_3, \text{mod}}$ do not follow standard scientific writing conventions. For guidance, you may refer to this document: <https://iupac.org/wpcontent/uploads/2016/01/ICTNS-On-the-use-of-italic-and-roman-fonts-for-symbols-in-scientific-text.pdf>*

We sincerely appreciate the reviewer's guidance on the proper use of italic and roman fonts for scientific symbols. Following the IUPAC recommendations, we have systematically revised the formatting of all symbols throughout the text and equations to ensure consistency with standard conventions.

3. *Line 217: Remove the dot after number 74.*

Done.

4. *Line 230: Using lighter background colors in Figure 1(a) would improve clarity and make the hotspots easier to distinguish.*

Thank you for the suggestion. We have redrawn Figure 1(a) using a lighter background color to enhance visual clarity and improve the distinction of hotspot regions.

5. *Line 235 and 245: Since these are comparative descriptions rather than time series trends, I'll avoid using "increase" and instead opt for terms like "overestimate" or "biases".*

Thank you for the helpful suggestion. We have revised the wording accordingly.

6. *Line 295: references for IPCC(2023)?*

We have added the appropriate reference for IPCC in the reference list.

7. *Line 351: Typos in this paragraph. Change SO_4^- to SO_4^{2-} .*

Corrected.

8. *line 505: References for the statement: "high-latitude marine aerosols are more acidic ..."?*

High-latitude marine aerosols are generally more acidic than those over remote ocean regions, primarily due to the long-range transport of anthropogenic pollutants such as H_2SO_4 and HNO_3 from continental sources. This enhanced acidity has been observed and simulated in several studies. For example, Karydis et al. (2021) conducted a global modeling study showing that aerosol pH in high-latitude marine regions is significantly influenced by anthropogenic outflow, particularly from Europe and North America. Similarly, Myhre et al. (2013) discuss how anthropogenic aerosols, including sulfate and nitrate, are transported to remote marine environments, altering their chemical composition and acidity. We have updated the text in the revised manuscript to include these references.

9. *Line 538: Table 9?*

We have corrected the table number accordingly.

10. *Line 539: It would be better to provide more context for the motivation of conducting the noNH₃ case earlier in the text-when introducing the cases in Table 1—rather than introducing it abruptly here.*

Thank you for the suggestion. We have added a brief explanation of the noNH₃ case in lines 176–180 to improve the flow of the manuscript.

11. *Line 556: Since the effects of different ammonia emission scheme are a crucial aspect of this research, and the title is "The Influence of Ammonia Emissions...", it would be more appropriate to move the sentences discussing the importance of the ammonia emission inventory and its effects earlier.*

We appreciate this thoughtful suggestion. After careful consideration, we have decided to retain the current structure to preserve the logical flow of the manuscript. Our approach begins with the model and observational datasets (Sections 2 and 3), followed by evaluation of the base case (Section 4), then analysis of global and regional aerosol chemical regimes (Sections 5 and 6), and finally the emission sensitivity analysis (Section 7). Reordering Section 7 earlier could disrupt this flow, as the interpretation of the emission scenario results depends on understanding the performance and limitations of the base case.

12. *Line 605: The figure captions for Figure 7 and Figure 8 are almost the same. You can change the caption of figure 8 to "The same as figure 7, but for the difference between Top-Dep case and base case.*

Thank you for the suggestion. We have revised the caption for Figure 8 accordingly.

References

350 Battaglia Jr, M. A., Weber, R. J., Nenes, A., and Hennigan, C. J.: Effects of water-soluble organic carbon
 on aerosol pH, *Atmos. Chem. Phys.*, 19, 14607-14620, 10.5194/acp-19-14607-2019, 2019.
 Guo, H., Xu, L., Bougiatioti, A., Cerully, K. M., Capps, S. L., Hite Jr, J. R., Carlton, A. G., Lee, S. H.,
 Bergin, M. H., Ng, N. L., Nenes, A., and Weber, R. J.: Fine-particle water and pH in the southeastern
 United States, *Atmos. Chem. Phys.*, 15, 5211-5228, 10.5194/acp-15-5211-2015, 2015.
 355 Karydis, V. A., Tsimpidi, A. P., Pozzer, A., and Lelieveld, J.: How alkaline compounds control atmospheric
 aerosol particle acidity, *Atmos. Chem. Phys.*, 21, 14983-15001, 10.5194/acp-21-14983-2021, 2021.
 Liu, M., Song, Y., Zhou, T., Xu, Z., Yan, C., Zheng, M., Wu, Z., Hu, M., Wu, Y., and Zhu, T.: Fine particle
 pH during severe haze episodes in northern China, *Geophysical Research Letters*, 44, 5213-5221,
 360 <https://doi.org/10.1002/2017GL073210>, 2017.
 Myhre, G., Samset, B. H., Schulz, M., Balkanski, Y., Bauer, S., Bernsten, T. K., Bian, H., Bellouin, N.,
 Chin, M., Diehl, T., Easter, R. C., Feichter, J., Ghan, S. J., Hauglustaine, D., Iversen, T., Kinne, S.,
 Kirkevåg, A., Lamarque, J. F., Lin, G., Liu, X., Lund, M. T., Luo, G., Ma, X., van Noije, T., Penner, J.
 E., Rasch, P. J., Ruiz, A., Seland, Ø., Skeie, R. B., Stier, P., Takemura, T., Tsigaridis, K., Wang, P., Wang,
 365 Z., Xu, L., Yu, H., Yu, F., Yoon, J. H., Zhang, K., Zhang, H., and Zhou, C.: Radiative forcing of the direct
 aerosol effect from AeroCom Phase II simulations, *Atmos. Chem. Phys.*, 13, 1853-1877, 10.5194/acp-
 13-1853-2013, 2013.
 Vasilakos, P., Russell, A., Weber, R., and Nenes, A.: Understanding nitrate formation in a world with less
 sulfate, *Atmos. Chem. Phys.*, 18, 12765-12775, 10.5194/acp-18-12765-2018, 2018.
 370

The influence of ammonia ~~emission~~emission inventories on the size-resolved global atmospheric aerosol composition and acidity

Xurong Wang¹, Alexandra P. Tsimpidi¹, Zhenqi Luo², Benedikt Steil³, Andrea Pozzer^{3,4}, Jos Lelieveld^{3,4}, and Vlassis A. Karydis¹

¹ Institute of Climate and Energy Systems: Troposphere (ICE-3), Forschungszentrum Jülich GmbH, Jülich, Germany

² School of Integrative Plant Science, Soil and Crop Sciences Section, Cornell University, Ithaca, NY 14853, United States of America

³ Max Planck Institute for Chemistry, Atmospheric Chemistry Dept., Mainz, Germany.

⁴ The Cyprus Institute, Climate and Atmosphere Research Center Nicosia, Nicosia, Cyprus.

Correspondence to:

Vlassis A. Karydis (v.karydis@fz-juelich.de, v.karydis@fz-juelich.de) and Alexandra P. Tsimpidi (a.tsimpidi@fz-juelich.de, a.tsimpidi@fz-juelich.de)

Abstract. Ammonia (NH₃) is an abundant alkaline gas in the atmosphere and a key precursor in the formation of particulate matter. While emissions of other aerosol precursors such as SO₂ and NO_x have decreased significantly, global NH₃ emissions are stable or increasing, and this trend is projected to continue. This study investigates the impact of NH₃ emission changes on size-resolved aerosol composition and acidity using the atmospheric chemistry-climate model EMAC. ~~Three~~Rather than directly perturbing NH₃ emissions, we employ three distinct emission schemes are analyzed in inventories: two bottom-up inventories and one derived using an updated top-down method. The results reveal that sulphate-nitrate-ammonium aerosols in two fine mode size ranges (0–1 µm and 1–2.5 µm) show the greatest sensitivity to NH₃ emission changes. Regional responses vary depending on the local chemical environment of secondary inorganic aerosols. In 'NH₃-rich' regions (e.g., East Asia and Europe), the abundance of NH₃ partially offsets the effects of reduced NH₃ emissions when NO_x and SO₂ are available, especially for aerosols in the 1–2.5 µm range. This highlights~~underscores~~ the importance of coordinated control strategies for NH₃, NO_x and SO₂ emissions. Further, we find that NH₃ has a buffering effect in densely populated areas, maintaining aerosol acidity at moderate levels and mitigating drastic pH shifts. ~~The study emphasizes that~~While pH changes are closely related to NH₃ emission variations, correlate strongly with the highest sensitivity observed NH₃ variability, they are also influenced by concurrent changes in the fine mode size ranges. SO₂ and NO_x emissions. These results highlight the critical role of NH₃ in shaping aerosol acidity ~~and argue, arguing~~ for size-specific approaches to managing particulate matter.

1. Introduction

As an abundant alkaline gas in the atmosphere, ammonia (NH₃) acts as a precursor in the formation of particulate matter by neutralizing atmospheric acids (e.g., H₂SO₄, HNO₃) to form sulfate-nitrate-ammonium (SNA) aerosols (Li et al., 2018; Chen et al., 2016; Wang et al., 2013), which are the main secondary inorganic components of PM_{2.5} (particulate matter with a diameter of 2.5 µm or less). By condensing onto freshly nucleated particles, NH₃ enhances

Formatted: Superscript

Formatted: Font: Italic

Formatted: Justified

Formatted: Font color: Auto

the growth rate of new particles as well as their hydrophilicity (Wang et al., 2020; Li et al., 2018). This can degrade air quality and change the solar radiative balance by interaction with radiation and clouds (Che et al., 2009; Zhao et al., 2011; Yao et al., 2018). In addition, the conjugate base-acid pair $\text{NH}_3/\text{NH}_4^+$ acts as the major buffer that inhibits changes in aerosol acidity (Chen et al., 2019; Zheng et al., 2020; Karydis et al., 2021).

Anthropogenic emissions are the main source of atmospheric NH_3 , with an average global contribution of 76%, dominated by agricultural activities, including livestock farming and the fertilization of soils (Schlesinger and Hartley, 1992; Dentener and Crutzen, 1994; Bouwman et al., 1997; Olivier et al., 1998; Van Aardenne et al., 2001; Bleeker et al., 2013). Meanwhile, the importance of non-agricultural sources, such as industrial emissions and fossil fuel combustion, has been highlighted by studies focusing on severe haze episodes in East Asia (Chang et al., 2019; Liu et al., 2018a; Pan et al., 2016). The construction of high-resolution regional or global datasets has characterized the spatiotemporal patterns of NH_3 emissions, with the most common datasets consisting of bottom-up inventories and top-down modeling inversion methods. Bottom-up emission inventories rely on activity data and emission factors, the latter being sensitive to assumptions about fertilizer types, local soil and meteorological properties (Bouwman et al., 2002; Sogaard et al., 2002; Xu et al., 2024). Zhang et al. (2018) evaluated discrepancies between bottom-up NH_3 emission inventories to exceed a factor of two, due to the uncertainties in emission factors, meteorological properties, and agricultural statistics (Beusen et al., 2008). Crippa et al. (2018) pointed out that the uncertainty in estimated NH_3 emissions is largest among all pollutants in the Emissions Database for Global Atmospheric Research (EDGAR v4.3.2), with a range of variation from 186% to 294% in 2012. In contrast, the ability of satellites to measure NH_3 abundance combined with numerical simulations allows a better characterization of the spatial distribution and seasonality of NH_3 emissions, but the low signal-to-noise ratio over low-emission areas limits the accuracy of retrieval products (Morán et al., 2016; Xu et al., 2016; Kong et al., 2019). Using a hybrid inverse modeling approach, Chen et al. (2021) optimized the NH_3 emission inventory NEI over the United States by combining CMAQ model simulations with constraints from the Infrared Atmospheric Sounding Interferometer (IASI) retrieval product. They found a 26% low bias of NH_3 emissions in the NEI, and the optimized NH_3 emission inventory improved the model performance of $\text{PM}_{2.5}$ mass concentration in the Midwest US, and the normalized mean bias of NH_4^+ and NO_3^- decreased from 27% to 22%, and 64% to 55%, respectively.

Recently, the emissions of SO_2 and NO_x have decreased due to the implementation of related clean air policies in East Asia, North America and Europe (Zheng et al., 2018; Hand et al., 2012; Russell et al., 2012; Aas et al., 2019; Gong et al., 2024), while the emissions of NH_3 remained stable or have slightly increased in major agricultural regions such as China (Xu et al., 2016), the United States (Yu et al., 2018), and Europe (Fortems-Cheiney et al., 2022). The increase in NH_3 emissions is associated with increasing fertilizer use and local temperatures (Warner et al., 2017; Xu et al., 2016; Skjøth and Geels, 2013; Xu et al., 2019), and such trends are expected to continue on a global scale throughout the century (IPCC, 2013). Driven by such emission ~~trend~~^{trends} of SO_2 , NO_x , and NH_3 , the main composition of SNA has changed in large regions with a shift from an ammonium sulfate to an ammonium nitrate formation regime (Tsimplidi et al., 2024; Lei et al., 2021; Jo et al., 2020; Zhou et al., 2019; Shah et al., 2018; Wang et al., 2013; Hauglustaine et al., 2014). Li et al. (2017) evaluated that during the period 1989 to 2013, the increasing trend of sulfate (SO_4^{2-}) and ammonium (NH_4^+) mass concentration in India and China occurred at a rate $>0.1 \mu\text{g m}^{-3}$

yr⁻¹, while decreasing trends were found in North America and Europe at a rate of about 0.1 µg m⁻³ yr⁻¹. The reduction of SO₂ and NO_x results in excess NH₃ being released to the atmosphere because less NH₃ is required to neutralize emissions, which decreases the atmospheric availability of H₂SO₄ and HNO₃, which in turn hinders the formation thereby reducing the demand for NH₃ to neutralize these acids and form particulate NH₄⁺. As NH₃ emissions have remained stable or slightly increased, this leads to an accumulation of NH₄⁺NH₃ in the aerosol/gas phase and increases the atmospheric NH₃ concentration (Liu et al., 2018b). Warner et al. (2017) assessed that the average increase rate of NH₃ mass concentration from 2002 to 2016 in the United States, Europe, and China was 2.6% yr⁻¹, 1.8% yr⁻¹, and 2.3% yr⁻¹, respectively. Some studies further pointed out that the increase in NH₃ concentration may offset the effectiveness of PM_{2.5} control achieved via SO₂ and NO_x emission reduction by promoting the formation of nitrate (NO₃⁻) (Huang et al., 2021; Cai et al., 2017; Zhang and Geng, 2019; Fu et al., 2017).

Several studies concluded that reducing NH₃ emissions would be a cost-effective way to control PM_{2.5} concentrations (Gu et al., 2021; Tsimpidi et al., 2007; Erisman and Schaap, 2004). However, the response of SNA to changes in its precursors is not linear (Pozzer et al., 2017; Wang et al., 2011; Wang et al., 2013; Tsimpidi et al., 2007; West et al., 1999), because the gas-particle partitioning of NH₃/NH₄⁺ and HNO₃/NO₃⁻ is influenced by several parameters, such as temperature, liquid water content, and aerosol acidity (Xu et al., 2020; Nenes et al., 2020; Guo et al., 2018). Nenes et al. (2020) developed a conceptual framework to describe the sensitivity of particulate matter to NO_x and NH₃ emissions, highlighting the critical influence of aerosol acidity and liquid water content on particulate matter formation. Based on sensitivity tests, Guo et al. (2018) evaluated that the response of NO₃⁻ to NH₃ reduction shows an apparent decrease only when the aerosol pH falls below the value of 3.

On the other hand, reductions in SO₂ and NO_x emissions are expected to reduce aerosol acidity, but recent studies revealed that aerosol acidity does not decrease as expected (Chen et al., 2019; Guo et al., 2017a; Zheng et al., 2022; Karydis et al., 2021). Aerosol acidity affects many processes involving the atmosphere and various aspects of the Earth system (Pye et al., 2020; Tilgner et al., 2021; Karydis et al., 2021) as well as human health (Dockery et al., 1993; Dockery et al., 1996; Thurston et al., 1994; Spengler et al., 1996). Weber et al. (2016) found that the acidity of PM_{2.5} in the southeastern United States remained at a relatively constant level with a pH value of 0 – 2 over the past 15 years, despite a 70% reduction in SO₄²⁻ concentration. A lack of aerosol acidity trend was also reported in China (Zhou et al., 2022). This is mainly caused by the buffering effect of NH₃/NH₄⁺ (Chen et al., 2019; Zheng et al., 2022; Zheng et al., 2020). To investigate this, Song et al. (2019) derived an equation from the partitioning of NH₃ and estimated that a unit increase in pH requires a tenfold increase in NH₃ concentration, which is consistent with the findings of Guo et al. (2017a). The regional variation of aerosol acidity is considerable, and the pH of PM_{2.5} in northern China is in the range of 4 to 5, which is higher than in Europe and the United States (Shi et al., 2019; Shi et al., 2017; Liu et al., 2017; Guo et al., 2015; Guo et al., 2016; Guo et al., 2017b; Karydis et al., 2021). This is caused by multiple driving factors, including aerosol mass concentration and composition, NH₃ mass concentration, aerosol water content, and meteorological factors (Ding et al., 2019; Zhang et al., 2021a). However, the main driver for the difference in aerosol acidity remains controversial. Zheng et al. (2020) pointed out that aerosol water content is the most important factor causing the regional variation of aerosol acidity, while Zhang et al. (2021a) emphasized the equal importance of aerosol mass concentration and chemical composition for the aerosol acidity contrasts between China and the United

Formatted: English (United States)

Formatted: English (United States), Not Superscript/ Subscript

485 States.

Almost all recent studies that discuss the response of aerosol composition and acidity to changes in NH₃ emission trends focus on the fine mode (e.g. PM_{2.5}). The size-resolved composition of SNA is not uniform (Karydis et al., 2016; Fang et al., 2017; Karydis et al., 2011; Karydis et al., 2010; Guo et al., 2017b), and NH₄⁺ and SO₄²⁻ are mainly concentrated in the fine mode (Wang et al., 2012; Seinfeld and Pandis, 2016), while NO₃⁻ aerosol can be formed on the surface of super-micron particles via heterogeneous chemistry (Allen et al., 2015). Furthermore, Milousis et al. (2024) revealed that the acidity of fine-mode aerosol is more sensitive to NH₃ emission than coarse-mode aerosol. Reducing the NH₃ emissions by half, the simulated pH of fine and coarse mode aerosol decreased by up to 3 and 1.5 units, respectively. Aerosol acidity tends to decrease with increasing particle size, with pH varying up to 6 units (Craig et al., 2018; Fang et al., 2017; Bougiatioti et al., 2016). Size-resolved aerosol acidity is associated with different formation pathways (Tilgner et al., 2021; Cheng et al., 2016). Ding et al. (2019) found that the coarse-mode aerosol shifted from neutral to weakly acidic with the increase of NO₃⁻ and SO₄²⁻ during severe hazy days. Cheng et al. (2016) further pointed out that the dominant oxidant in SO₄²⁻ production by SO₂ oxidation changes with the ambient aerosol acidity. Therefore, it is necessary to comprehensively investigate the response of size-resolved chemical composition and acidity to changes in NH₃ emissions.

500 In this study, ~~three different we investigate the influence of ammonia (NH₃ emission schemes are used as input to the atmospheric chemistry climate model) emissions on size-resolved aerosol composition and acidity using the EMAC (ECHAM5/MESSy Atmospheric Chemistry). The three emission schemes include two bottom-up model. The EMAC model, coupled with the ISORROPIA-II thermodynamic module, provides a robust framework for simulating global aerosol-chemistry-climate interactions and estimating aerosol pH under varying environmental conditions. Rather than directly perturbing NH₃ emissions, we employ three distinct emission inventories: two bottom-up inventories (CAM5 and CEDS_GBD) and one derived using an updated emission inventory produced following a top-down method approach (Luo et al., 2022). Satellite retrievals of NH₃ column concentrations and aerosol composition observational datasets from multiple sites around the world are used to evaluate the aerosol simulations derived from these scenarios allow us to assess the three NH₃ emission schemes. We investigate the responsesensitivity of size-resolved aerosol SNA composition and acidity to changes aerosols to realistic variations in NH₃ emissions across three well-characterized, anthropogenically polluted regions in the Northern Hemisphere. These regions, representing a gradient from relatively less to more polluted conditions, include the United States, in conjunction with co-varying SO₂ and NO_x trends. Model results are evaluated against satellite-derived NH₃ columns and ground-based aerosol composition observations. Our analysis spans four aerosol size ranges (0–1 μm, 1–2.5 μm, 2.5–5 μm, and 5–10 μm) and includes regional assessments over North America, Europe, and the North China Plain. The examined aerosol sizes range (diameter) from sub-micron (0–1 μm) to super-micron (1–2.5 μm, 2.5–5 μm, and 5–10 μm). East Asia to explore chemical regime shifts and buffering capacity.~~

2. Modelling description

520 EMAC (ECHAM5/MESSy) is a global atmospheric chemistry and climate model, which includes a number of submodels describing atmospheric processes and interactions among oceans, land, and anthropogenic influences

Formatted: English (United Kingdom)

Formatted: English (United Kingdom)

Formatted: English (United Kingdom)

Formatted: English (United Kingdom)

Formatted: English (United Kingdom)

Formatted: English (United Kingdom)

Formatted: English (United Kingdom)

Formatted: English (United Kingdom)

Formatted: English (United Kingdom)

Formatted: Font: +Body (Aptos)

Formatted: English (United Kingdom)

Formatted: English (United Kingdom)

Formatted: English (United Kingdom)

Formatted: English (United Kingdom)

Formatted: English (United Kingdom)

(Jöckel et al., 2016). These submodels are linked to the base model, the 5th generation European Centre Hamburg general circulation model (ECHAM5; Roeckner et al., 2006), via the Modular Earth Submodel System (MESSy; Jöckel et al., 2005). In this study, the horizontal resolution of the EMAC model is T63L31, which corresponds to a grid resolution of about $1.875^\circ \times 1.875^\circ$ (Jöckel et al., 2010) and 31 vertical layers extending up to 25 km altitude. EMAC is applied for 4 years, from 2009 to 2012 with the first year used as a spin-up. The meteorological reanalysis data ERA5 (Hersbach et al., 2020), with a significantly enhanced horizontal resolution of 31km and hourly output throughout, is used in EMAC to nudge the simulation.

In EMAC, organic aerosol (OA) formation is simulated by the ORACLE module (Tsimpidi et al., 2014; Tsimpidi et al., 2016), where logarithmically spaced saturation concentration bins are used to describe the organic aerosol components based on their volatility. The aerosol microphysics and gas/aerosol partitioning are calculated by the Global Modal-aerosol eXtension (GMXe) module described by Pringle et al. (2010), which has the same microphysical core as the M7 sub-model (Vignati et al., 2004). The aerosol size distribution is treated by 7 log-normal modes, including 4 hydrophilic and 3 hydrophobic modes, covering nucleation (soluble only), Aitken, accumulation, and coarse modes (both soluble and insoluble). To determine size-resolved aerosol composition and pH, we sum the contributions of each aerosol component, water content, and H^+ concentration across all GMXe modes corresponding to a given size range. This is achieved by calculating the volume fraction of the lognormal distribution of each mode that falls within the specified size limits. The atmospheric chemistry module MECCA (Module Efficiently Calculating the Chemistry of the Atmosphere), which contains a comprehensive atmospheric reaction is used to calculate the gas concentrations (Sander et al., 2019). The SEDI module is used to compute aerosol particle sedimentation (Kerkweg et al., 2006). Dry deposition and wet deposition of gas and particle species are calculated by the DRYDEP module (Kerkweg et al., 2006) and the SCAV module (Tost et al., 2006), respectively. The CLOUD submodel (Roeckner et al., 2006) is used to calculate cloud properties and microphysics, utilizing the microphysical scheme of Lohmann and Ferrachat (2010) and a physically based treatment of liquid (Karydis et al., 2017) and ice crystal (Bacer et al., 2018) activation processes.

An advanced parameterization scheme is incorporated into the EMAC model to calculate the dust emission flux online (Astitha et al., 2012). The scheme uses the online meteorological fields from the EMAC model, such as temperature, pressure, relative humidity, soil moisture, and surface friction velocity, to calculate the threshold friction velocity which is the initial step of dust production. Above the threshold friction velocity, dust emission is possible. Following Karydis et al. (2016), the emissions of individual crustal species in this study are estimated as constant fractions of the dust emission (Klingmüller et al., 2018). These fractional factors depend on the geological information, which includes different dust emission sources. Karydis et al. (2021) pointed out that the crustal ions (Ca^{2+} , Mg^{2+} , K^+ , and Na^+), especially Ca^{2+} , have significantly contributed to maintaining the particle pH value at the level of 4.5 – 5 in East Asia during the last decade. The importance of crustal ions in determining aerosol acidity and factors such as liquid water content, aerosol mass concentration, and chemical composition, has been highlighted in other studies (Zheng et al., 2020; Zhang et al., 2021a; Ding et al., 2019).

2.1 NH₃ emission scheme

In this study, three NH₃ emission schemes are applied in specific model simulation cases to quantify the impact of changes in NH₃ emissions on aerosol composition and acidity (Table 1). These include two bottom-up inventories used in the Base and Top-CEDS cases, and one top-down scheme inventory applied in the Top-Dep case. In addition, two sensitivity simulations are conducted: the Meta case, which assumes metastable aerosol thermodynamics (described in detail in Section 2.2), and the noNH₃ case, in which all NH₃ emissions are turned off. The latter is used to provide insights into the role of NH₃ in shaping the simulated size-resolved aerosol acidity.

Table 1. Overview of simulation cases.

Simulation Case	NH ₃ Emission Scheme	Equilibrium State
Base	CAMS-GLOB-ANT, CAMS-GLOB-AIR, GEIA, biomass burning	Stable
CEDS	Same as Base case, but NH ₃ , SO ₂ , and NO _x are from CEDS-GBD	Stable
Top-Dep	Luo's method with the lifetime derived from deposition, GEIA-water	Stable
Meta	Same as Base case	Metastable
noNH ₃	No NH ₃ emission input	Stable

2.1.1 Bottom-up scheme

Bottom-up schemes are applied in the base and the CEDS cases, with different anthropogenic emission inventories. The anthropogenic emission inventory utilized in the base case simulation is CAMS-GLOB-ANT (v4.2, <https://eccad3.sedoo.fr>, abbreviated as "CAMS"), which contains 17 sectors with a spatial resolution of 0.1 × 0.1 degree and monthly temporal resolution. With the basic data of 2010 from the Emission Database for Global Atmospheric Research (EDGAR, v4.3.2), CAMS extends the period to recent years based on the trend factors derived from the Community Emissions Data System (Hoesly et al., 2018). Meanwhile, Hoesly et al. (2018) pointed out that there are limitations in the system, especially in the emission trends for specific sectors, and emphasized the need for more detailed data to be incorporated into regional emission inventories. The other one used in the CEDS sensitivity simulation case for aerosol precursor emissions (NH₃, SO₂, and NO_x) is CEDS-GBD-MAPS (McDuffie et al., 2020), abbreviated as "CEDS_GBD". The CEDS_GBD is developed using the Community Emissions Data System and is reported as a function of 11 anthropogenic sectors and 4 fuel categories, with a spatial resolution of 0.5 × 0.5 degrees and monthly temporal resolution. Assuming that the specific regional emission inventories are more accurate, McDuffie et al. (2020) updated the activity data and the core scaling procedure, modified the final emission gridding and aggregation procedures, and then utilized several regional emission inventories to improve the previous version of CEDS_GBD via the scaling procedure, which can not only reduce the discrepancy with other global emission inventories but also help to maintain the timeliness and regional accuracy of the global estimates. However, they also pointed out that the sources of uncertainty in the CEDS_GBD are similar to those in the CEDS.

Other NH₃ emissions include aircraft emissions from the CAMS-GLOB-AIR inventory (v1.1, <https://eccad3.sedoo.fr>), land and water biological emissions from the Global Emissions Inventory Activity (GEIA) inventory, and biomass burning emissions calculated by the BIOBURN submodel (Kaiser et al., 2012). BIOBURN determines the flux based on biomass burning emission factors and dry matter combustion rates from the Global Fire Assimilation System (GFAS), which calculates biomass burning emissions by assimilating Fire Radiative

Formatted: English (United States)

Formatted: No underline, Font color: Auto

Power (FRP) observations from MODIS (Andreae, 2019).

2.1.2 Top-down scheme

The NH₃ emission inventory over land is updated by a top-down method with the constraint of IASI satellite observations (<https://iasi.aeris-data.fr>) developed by Luo et al. (2022). This fast top-down method updates the prior NH₃ emissions ($E_{NH_3,mod}$, molecule m⁻² s⁻¹) with a correction term positively proportional to the biases between observed ($C_{NH_3,obs}$, molecule m⁻²) and simulated ($C_{NH_3,mod}$, molecule m⁻²) monthly averaged NH₃ total column densities and inversely proportional to the NH₃ lifetime ($\tau_{NH_3,mod}$, s) (Eq. 1). The $\tau_{NH_3,mod}$ is calculated as the ratio of the simulated NH₃ column and the sum of the simulated loss rate of the NH_x family (NH_x ≡ NH₃+ NH₄⁺) through dry and wet deposition (Eq. 2).

$$E_{NH_3} = E_{NH_3,mod} + \frac{C_{NH_3,obs} - C_{NH_3,mod}}{\tau_{NH_3,mod}} E_{NH_3} = E_{NH_3,mod} + \frac{C_{NH_3,obs} - C_{NH_3,mod}}{\tau_{NH_3,mod}} \quad (1)$$

$$\tau_{NH_3,mod} = \frac{C_{NH_3,mod}}{D_{NH_3,mod} + D_{NH_4^+,mod}} \tau_{NH_3,mod} = \frac{C_{NH_3,mod}}{D_{NH_3,mod} + D_{NH_4^+,mod}} \quad (2)$$

The fast top-down method relies on the total column concentrations retrieved by IASI. According to Dammers et al. (2019), the dominant source of uncertainty in the IASI observational product stems from the systematic bias, with the negative bias estimated between 25% to 40%, compared to site observations (Dammers et al., 2017). While this method simplifies the chemical and physical processes governing NH₃, Luo et al. (2022) identified large uncertainties in regions like Central Asia and tropical Africa due to poorly constrained sources by IASI observations in these areas. Nonetheless, they demonstrated that simulations driven by the updated top-down emission inventory show better consistency with satellite observations compared to those driven by the prior emission inventory.

2.1.3 Emission comparison

Overall, the global NH₃ emissions used in this study in all simulation cases range from 74.73 Tg yr⁻¹ to 85 Tg yr⁻¹ (Table 2), which is within the reported range of the current literature from 52 Tg yr⁻¹ to 91 Tg yr⁻¹ (Schlesinger and Hartley, 1992; Dentener and Crutzen, 1994; Bouwman et al., 1997; Olivier et al., 1998; Van Aardenne et al., 2001; Bleeker et al., 2013). The distribution of the global NH₃ emission flux derived from the base case and the absolute emission flux difference between the sensitivity simulation cases and the base case are shown in Figure 1. Significant regional variations in NH₃ emission flux are found in Figure 1(a), with the maximum emission flux exceeding 7 g m⁻² yr⁻¹ in northern India, eastern China, and central Europe, all regions with the highest population density. Other emission hotspots include the eastern United States, southeastern Latin America, and central and eastern Africa. The base case is able to capture the global NH₃ emission hotspots reported by Van Damme et al. (2018). Meanwhile, the minimum flux below 0.01 g m⁻² yr⁻¹ is located in the Antarctic and Arctic regions and the Sahara Desert, as well as in remote oceans, where there is little impact from human activities. Agricultural activities including livestock and

Formatted: Subscript

fertilization are the main source of NH_3 emissions in China, India, and the United States (Liu et al., 2022; Khan et al., 2020; Van Damme et al., 2018; Sahoo et al., 2024), while soil emissions, biomass burning and domestic fires are the main contributors to NH_3 emissions in central and eastern Africa (Hickman et al., 2021; Delon et al., 2012).

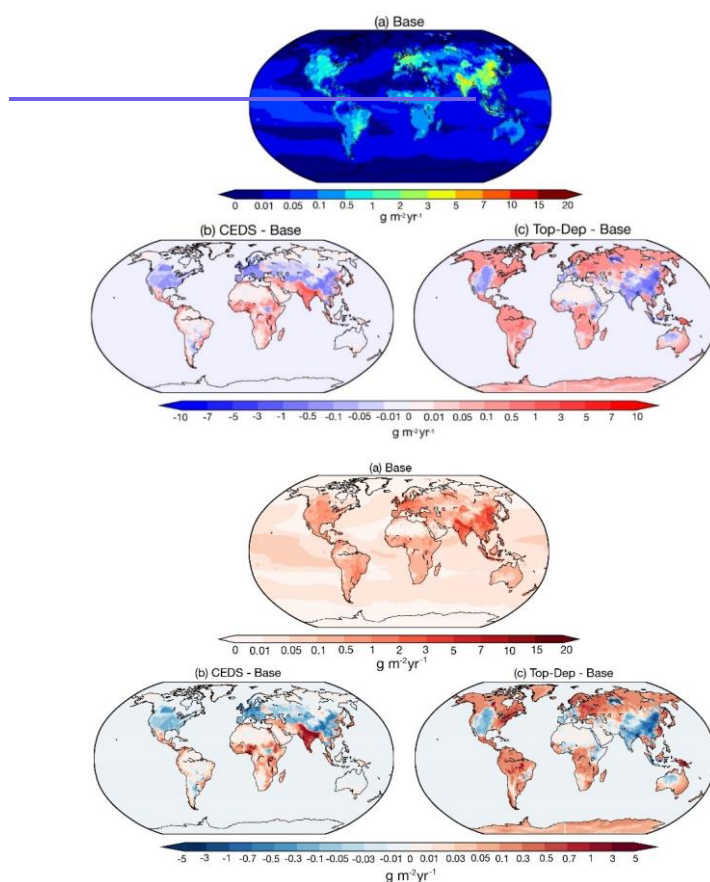


Figure 1. Global distribution of the annual average NH_3 emission flux for (a) the Base case and the absolute differences between (b) the Base and CEDS and (c) the Base and Top-Dep cases during 2010–2012.

Compared with the base case, the global NH_3 emissions in both the CEDS and Top-Dep cases show an increase exceed those in the global NH_3 emission amount base case, with increases of approximately 5% and 16%, respectively. The lower NH_3 emission fluxes of the CEDS case are found in North America, Europe, and China except for the northeastern and southeastern coastal areas, while emission fluxes are higher throughout India (Figure 1b). Slightly higher fluxes are also found in western and eastern Africa, the northern Middle East, and southeastern Asia.

According to Meduffie et al. (2020), the NH₃ emission flux from the Multi-resolution Emission Inventory for China (MEIC, <http://www.meicmodel.org>), European Monitoring and Evaluation Programme (EMEP), and US EPA are used to scale the previous emission (the basic data of 2010 from EDGAR) over mainland China, Europe, and the USA. The NH₃ emission flux from India and Africa remains the same as that of the original inventory. Constrained by the IASI satellite observation, the NH₃ emission flux of the Top-Dep case is ~~increased~~^{elevated} in most regions of the world, but lower emission fluxes are estimated in regions such as western North America, western and southern Europe, India, China except the northeastern and southeastern coastal areas, and western Australia. The comparison of the absolute and relative difference between the base case and the other emission schemes is summarized in Table 2.

Table 2. Comparison of annual NH₃ emissions (Tg yr⁻¹) across global and regional scales between the two sensitivity cases ~~cases~~ and the base case.

Region	Base (Tg yr ⁻¹)	diff ^a	CEDS relative diff ^b (%)	diff ^a	Top-Dep relative diff ^b (%)
Globe	73.273	3.869	5.3	11.444	16
Land	61.441	3.050	5.0	11.263	18
North America	5.566	-1.000	-18	3.232	58
South America	8.202	0.697	8.4	4.482	51
Europe	6.444	-1.505	-23	1.010	16
Middle East	1.051	0.242	20	-0.01 ^c	-1.4
South Asia	10.441	3.798	38	-1.098	-9.7
East Asia	15.757	-2.030	-13	-2.586	-16

^a: absolute difference between sensitivity cases and the base case.

^b: relative difference between sensitivity cases and the base case.

^c: below the 0.1 precision threshold.

2.2 ISORROPIA II

The thermodynamic equilibrium model ISORROPIA II is used to calculate the multi-phase mass transfer of the K⁺-Ca²⁺-Mg²⁺-NH₄⁺-Na⁺-SO₄²⁻-NO₃⁻-Cl⁻-H₂O aerosol system (Nenes et al., 1998; Fountoukis and Nenes, 2007). The process of gas/aerosol partitioning is calculated in two steps (Pringle et al., 2010). In the first step, the amount of gas phase species kinetically able to condense on the aerosol within one timestep is calculated (Vignati et al., 2004). ISORROPIA II then re-distributes the mass between the gas and aerosol phase. In this study, ISORROPIA II runs in the forward mode with the input of relative humidity, temperature, and concentration of aerosol and gas phase species. ISORROPIA II determines the subsystem set of equilibrium equations and solves the equilibrium state by the chemical potential method. It outputs the equilibrium concentration of species in gas, solid, and liquid phases by assuming that the particle phase is in the thermodynamically stable-state mode where salts precipitate once the aqueous phase becomes saturated (Fountoukis and Nenes, 2007).

Meanwhile, a sensitivity case assuming the particle phase in the thermodynamically metastable state mode is performed with the same emission scheme as the base case. (*Meta case*). In the metastable state, the aerosol may be supersaturated with respect to dissolved salts and always consists only of an aqueous phase (Fountoukis and Nenes, 2007). Karydis et al. (2021) pointed out that more acidic particles (up to 2 pH units) are derived from the metastable assumption in regions affected by high concentrations of crustal cations and consistently low relative humidity values.

According to past studies, the treatment of crustal species (e.g. Ca²⁺, K⁺, Mg²⁺) in ISORROPIA II can improve model predictions (Karydis et al., 2010; Karydis et al., 2011), as both the phase partitioning of NO₃⁻ and the

Formatted Table

thermodynamic interaction between NH_4^+ and the remaining ions in the aqueous phase are significantly affected. Karydis et al. (2016) found that when these crustal species are included in the EMAC model, the increase in global NO_3^- tropospheric load can be up to 44% while the global NH_4^+ tropospheric load decreases by 41%.

Formatted: English (United Kingdom)

2.2.1 pH calculations

The pH is calculated from the negative decimal logarithm of the hydrogen ion activity,

$$\text{pH} = -\log_{10} \text{pH} = -\log_{10}(\gamma x_{\text{H}^+} x_{\text{H}^+}) \quad (3)$$

where x_{H^+} and γ represent the molality of hydrogen ions in the solution and the ionic activity coefficient of hydrogen, respectively. With γ assumed to be unity, the pH value is derived using the hydrogen ion concentration in the aqueous particle phase output by ISORROPIA-II (in mol m^{-3}) and the aerosol water content output by GMXe (in mol mol^{-1}). The effect of water-soluble organic aerosols on aerosol water content is accounted for via the GMXe module, which includes both inorganic and organic contributions. Organic aerosol formation is simulated using the ORACLE module, and the associated water uptake is calculated assuming a κ -hygroscopicity value of 0.14 for all organic components (Tsimpidi et al., 2017). This influences the total aerosol water content used in pH calculations. Both hydrogen ion and aerosol water content are output every 5 hours, following Karydis et al. (2021). In addition, the temperature threshold of 269 K is set to ensure that the calculations are performed only when liquid water is present in the aerosol.

Formatted: English (United States)

Formatted: English (United States)

Formatted: English (United States)

Formatted: Font: Italic

Formatted: English (United States)

Formatted: Font: Italic

Formatted: English (United States)

Formatted: English (United States)

Formatted: English (United States)

Formatted: English (United States)

Discrepancies among thermodynamic models tend to increase as RH decreases, primarily due to differing assumptions about activity coefficients (Pye et al., 2020). ISORROPIA-II assumes constant mean activity coefficients and a unity activity coefficient for H^+ , which results in relatively invariant and often lower pH predictions under dry conditions. Additionally, the choice between stable and metastable phase state assumptions introduces further uncertainty. Under low RH (e.g., <35%), the metastable assumption allows for supersaturated solutions, enabling pH calculations even at low aerosol liquid water content, often resulting in low pH values. Conversely, the stable state permits salt crystallization, and in cases where the aerosol becomes fully solid, pH may no longer be defined. To assess the sensitivity of our results to this assumption, we conducted a simulation using the metastable assumption (Meta case; see Table 1).

EMAC model does not account for chemical interactions between ammonia and organic acids (e.g., ammonium oxalate formation) and treats inorganic and organic aerosol phases separately. As a result, while organics can indirectly influence pH through their contribution to aerosol water content, changes in NH_3 emissions do not affect organic aerosol formation or the associated water content in our simulations. Furthermore, although the influence of organics on hydrogen ion activity coefficients is not explicitly represented, previous studies have shown that water-soluble organic aerosols exert only a minor effect on aerosol pH (Guo et al., 2015; Pye et al., 2018; Vasilakos et al., 2018).

2.2.2 Two factors affecting pH value change

According to Equation (3), the pH value is determined by the concentrations of H^+ and H_2O . To evaluate the impact of each factor on the pH value, we independently calculate the changes in pH arising from two pathways: one driven by H^+ and the other by H_2O . The corresponding results are presented in Figures S16 and S17.

$$\Delta pH_{H_2O} = \log_{10} \frac{H_2O + \Delta H_2O}{H_2O} - \log_{10} \frac{H_2O}{H^+} - \log_{10} \frac{H_2O}{H^+} \quad (4)$$

$$\Delta pH_{H^+} = \log_{10} \frac{H^+ + \Delta H^+}{H^+} - \log_{10} \frac{H^+}{H_2O} - \log_{10} \frac{H^+}{H_2O} \quad (5)$$

Here, ΔpH_{H_2O} and ΔpH_{H^+} represent the changes in pH caused by variations in H_2O and H^+ concentrations, respectively. The base case concentrations of H_2O and H^+ are used as references, and the changes in concentration are expressed as ΔH_2O and ΔH^+ , corresponding to the deviations in H_2O and H^+ from their base case levels.

3. Observations

Multiple observational datasets are used in this study to validate the model simulation in different regions of the world as defined by the IPCC (2023/2022). The information of each dataset is summarized in Table 3 and the site distribution is plotted in Figure 2 and Figure S1. These datasets include satellite retrievals from the Infrared Atmospheric Sounding Interferometer (IASI; https://iasi.aeris-data.fr/NH3_IASI_A_L3_data/), and observation site networks Nationwide Nitrogen Deposition Monitoring Network (NNDMN; https://figshare.com/articles/dataset/Data_Descriptor_Xu_et_al_20181211_Scientific_data_docx/7451357/5), the European Monitoring and Evaluation Programme (EMEP; <https://ebas-data.nilu.no/Default.aspx>), the Central Pollution Control Board (CPCB; <https://cpcb.nic.in/>), the Acid Deposition Monitoring Network in East Asia (EANET; <http://www.eanet.asia/product/index.html>), Ammonia Monitoring Network (AMoN; <https://nadp.slh.wisc.edu/networks/ammonia-monitoring-network/>), the U.S. Environmental Protection Agency (EPA; <https://www.epa.gov/data>), and the Clean Air Status and Trends Network (CASTNET; <http://www.epa.gov/castnet>).

Table 3. Information for each observation dataset used to validate model simulation during 2010–2012.

Dataset	Parameters	Location
IASI	NH ₃ column concentration	Globe ^a
NNDMN	NH ₃ , NH ₄ ⁺ , NO ₃ ⁻ mass concentration	China (29 sites)
EMEP	NH ₃ , NH ₄ ⁺ , NO ₃ ⁻ , and SO ₄ ²⁻ mass concentration	Europe (25 sites for NH ₃ ; 7 sites of PM _{2.5} matrix ^b)
CPCB	NH ₃ mass concentration	India (8 sites)
EANET	NH ₄ ⁺ , NO ₃ ⁻ , and SO ₄ ²⁻ mass concentration	eastern and southeastern Asia (50 sites, PM _{2.5} matrix ^b)
AMoN	NH ₃ and NH ₄ ⁺ mass concentration	America (21 sites)
CASTNET	NH ₃ , NH ₄ ⁺ , NO ₃ ⁻ , and SO ₄ ²⁻ mass concentration	America (79 sites, PM _{2.5} matrix ^b)
EPA	NH ₄ ⁺ , NO ₃ ⁻ , and SO ₄ ²⁻ mass concentration	America (211 sites, PM _{2.5} matrix ^b)

^a: Only use the data over land.

^b: Measurements refer to a chemical or physical property of the total aerosol particle phase in the size fraction less than 2.5 micrometer median aerodynamic diameter.

Due to its better precision resulting from favorable thermal contrast conditions (Clarisse et al., 2009), only the

morning (around 9:30 local time) overland IASI data is used in this study. The original temporal resolution of the various datasets includes hourly, three-day, daily, weekly, bi-weekly, and monthly, which we uniformly convert to monthly. The mean bias (MB), mean absolute gross error (MAGE), normalized mean bias (NMB), normalized mean error (NME), and root mean square error (RMSE) are calculated to evaluate the model performance:

$$MAGE = \frac{1}{N} \sum_{i=1}^N |P_i - O_i| \quad (6)$$

$$MB = \frac{1}{N} \sum_{i=1}^N (P_i - O_i) \quad (7)$$

$$NME = \frac{\sum_{i=1}^N |P_i - O_i|}{\sum_{i=1}^N O_i} \quad (8)$$

$$NMB = \frac{\sum_{i=1}^N (P_i - O_i)}{\sum_{i=1}^N O_i} \quad (9)$$

$$RMSE = \left[\frac{1}{N} \sum_{i=1}^N (P_i - O_i)^2 \right]^{\frac{1}{2}} \quad (10)$$

where P_i and O_i represent the monthly value of model simulation and measurement, respectively. N is the total number of data points used for comparison.

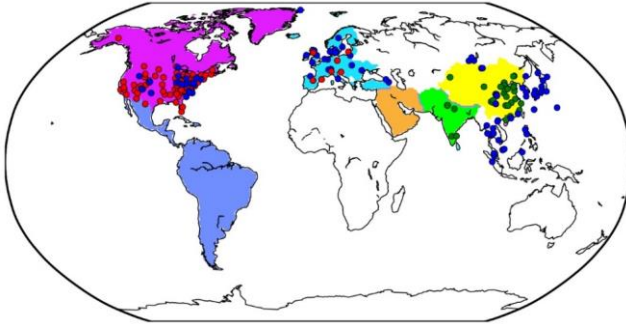


Figure 2. Regions and observation sites used in this study. North America, South America, Europe, Middle East, South Asia, and East Asia are marked represented by purple, navy blue, sky blue, orange, light green, and yellow, respectively. In North America AMoN and CASTNET sites are represented by shown as blue and red circles in North America (the, respectively (EPA sites are shown provided in Figure S3-S1). In Europe, EMEP sites in Europe are shown by blue circles for NH₃ and red circles for PM_{2.5} components. In South Asia, CPCB sites are marked by green circles in South. In East Asia, while NNDMN and EANET sites are indicated by dark green and dark blue in East Asia circles, respectively.

4. Observation Model evaluation

4.1 Aerosol comparison composition

The comparison between the simulation derived from the base case and the observational datasets is summarized in Tables 4 – 6. Compared with the NNDMN dataset, of which primarily includes sites are mainly located in urban and rural areas of across China, the base case overestimates the NH₃ mass concentration (NMB = 0.19), underestimates the NH₄⁺ mass concentration (NMB = -0.41) though reproduces the NO₃⁻ mass concentration well (NMB = -0.02).

Xie et al. (2022) summarized the NMB between observed NO_3^- and simulated values in China as ranging from -0.97 to 1.90 based on modelling studies in the last decade. The negligible bias of the simulated NO_3^- shows the good performance of the EMAC model in this region. However, the biases in the simulation of NH_3 and NH_4^+ indicate that the $\text{NH}_3/\text{NH}_4^+$ partitioning treatment is not efficient enough or over-simplified, as less NH_4^+ is produced even with sufficient NH_3 . Similarly, in Europe and North America, we obtain a positive bias of NH_3 mass concentration (EMEP dataset: NMB = 2.26; AMoN dataset: NMB = 0.58) and a comparably lower NH_4^+ mass concentration (EMEP dataset: NMB = 0.05; AMoN dataset: NMB = -0.23). On the other hand, the dry deposition of NH_3 in China is lower than reported from observations (NMB = -0.28; not shown), which contributes to a higher atmospheric NH_3 concentration.

Table 4. Comparison of the Base case predictions with monthly average observations from China and Europe during 2010–2012.

	NNDMN network <i>Metrie</i>			EMEP network <i>Metrie</i>			
	NH_3	NH_4^+	NO_3^-	NH_3	NH_4^+	NO_3^-	SO_4^{2-}
Observed ($\mu\text{g m}^{-3}$)	7.68	7.45	11.92	1.16	1.09	1.29	2.11
Simulated ($\mu\text{g m}^{-3}$)	9.14	4.40	11.70	3.79	1.15	3.33	1.24
MAGE ($\mu\text{g m}^{-3}$)	5.27	4.21	6.00	2.78	0.60	2.38	0.98
MB ($\mu\text{g m}^{-3}$)	1.46	-3.05	-0.22	2.63	0.06	2.04	-0.88
NME	0.69	0.56	0.50	2.40	0.55	1.84	0.46
NMB	0.19	-0.41	-0.02	2.26	0.05	1.58	-0.41
RMSE ($\mu\text{g m}^{-3}$)	7.43	6.55	9.07	4.03	0.97	2.95	1.63
Number of comparisons	765	765	765	832	249	320	320

Table 5. Comparison of the Base case predictions with monthly average observations from India and eastern Asia (PM_{25} matrix) during 2010–2012.

	CPCB network <i>Metrie</i>	EANET network <i>Metrie</i>		
	NH_3	NH_4^+	NO_3^-	SO_4^{2-}
Observed ($\mu\text{g m}^{-3}$)	30.07	0.84	1.22	2.95
Simulated ($\mu\text{g m}^{-3}$)	22.30	0.83	2.09	1.52
MAGE ($\mu\text{g m}^{-3}$)	21.25	0.55	1.58	1.74
MB ($\mu\text{g m}^{-3}$)	-7.78	-0.02	0.87	-1.43
NME	0.71	0.65	1.29	0.59
NMB	-0.26	-0.02	0.71	-0.49
RMSE ($\mu\text{g m}^{-3}$)	30.57	1.11	2.58	2.48
Number of comparisons	137	908	916	886

Table 6. Comparison of the Base case predictions with monthly average observations from America (PM_{25} matrix) during 2010–2012.

	AMoN network <i>Metrie</i>		CASTNET network <i>Metrie</i>			EPA network <i>Metrie</i>		
	NH_3	NH_4^+	NH_4^+	NO_3^-	SO_4^{2-}	NH_4^+	NO_3^-	SO_4^{2-}
Observed ($\mu\text{g m}^{-3}$)	1.20	1.27	0.69	0.74	1.81	0.83	1.24	1.97
Simulated ($\mu\text{g m}^{-3}$)	1.89	0.99	0.90	1.96	1.34	1.02	2.22	1.44
MAGE ($\mu\text{g m}^{-3}$)	1.16	1.02	0.34	1.33	0.64	0.42	1.30	0.65
MB ($\mu\text{g m}^{-3}$)	0.69	-0.29	0.21	1.22	-0.46	0.19	0.98	-0.53
NME	0.97	0.80	0.49	1.80	0.36	0.51	1.05	0.33
NMB	0.58	-0.23	0.30	1.65	-0.26	0.23	0.79	-0.27
RMSE ($\mu\text{g m}^{-3}$)	1.64	1.43	0.45	1.71	0.86	0.60	1.76	0.90
Number of comparisons	553	552	2825	2825	2825	5085	5392	5429

In East and Southeast Asia, the mass concentration of NH_4^+ is well reproduced (NMB = -0.02), while high and low discrepancies are found in the mass concentrations of NO_3^- and SO_4^{2-} (NMB = 0.71 and -0.49, respectively). Similar results were also found in Europe, with agreement for NH_4^+ (NMB = 0.05) but an overestimation of the NO_3^- mass

concentration (NMB = 1.58) and underestimated SO_4^{2-} (NMB = -0.41). The positive bias of the simulated NO_3^- is reported by many studies (Xie et al., 2022; Heald et al., 2012; Colette et al., 2011; Bian et al., 2017; Pozzer et al., 2022; Milousis et al., 2025). The negative bias of SO_4^{2-} is considered a reason for the positive bias of NO_3^- , regarding the thermodynamic equilibrium between NH_4^+ , $\text{SO}_4\text{SO}_4^{2-}$, and NO_3^- . The discrepancy in $\text{SO}_4\text{SO}_4^{2-}$ and NO_3^- is also due to the missing heterogeneous oxidation reactions for SO_2 and NO_x in the model. Several studies have concluded that adding multiphase chemistry can significantly improve the model performance (Zheng et al., 2015; Zhang et al., 2021b). Cheng et al. (2016) and Zheng et al. (2024) pointed out that the multiphase reactions act as an important SO_4^{2-} source in haze pollution, while Guo et al. (2017a) argued that the multiphase reactions are not likely limited by the required alkaline environment.

In North America, the base case reproduces the mass concentration of SO_4^{2-} (NMB = -0.26), but overpredicts the mass concentrations of NH_4^+ and NO_3^- (NMB = 0.23 and 0.79, respectively), which is in line with the findings of Walker et al. (2012). The excess NH_4^+ promotes the formation of NO_3^- , and the uncertain uptake coefficient of N_2O_5 used in models may contribute to more NO_3^- (Walker et al., 2012). The highest NH_3 mass concentration is found in India, especially in the Indo-Gangetic Plain. Our model basically captures the “hot spot”, with a slight negative bias (NMB = -0.26). However, the scarce observation sites and the lack of observed NH_4^+ , NO_3^- and SO_4^{2-} hinder further evaluation of the model performance.

4.2 pH-value comparison Aerosol acidity

Due to the lack of direct measurement of aerosol acidity, we collect the $\text{PM}_{2.5}$ pH value from related studies to compare with our model simulation in Table 7. These pH values are calculated using the thermodynamic equilibrium model ISORROPIA or E-AIM with input from observational datasets. Compared with Guo et al. (2017b), our simulated pH value from the base case is higher in the western USA (4.3 vs 2.7), but the value from the Meta case is much closer (2.6). Both the base and Meta cases predict the same aerosol water content, and the high Ca^{2+} concentration from the Great Basin Desert leading to the precipitation of CaSO_4 is the main reason for the lower aerosol acidity in the base case (Karydis et al., 2021). It is worth noting that the effect of Ca^{2+} on aerosol acidity was not considered by Guo et al. (2017b). The summertime southeastern USA is characterized as relatively clean with aerosol dominated by NH_4^+ and SO_4^{2-} , but negligible mineral cations, the aerosol is acidic with the observed pH value around ~0.6 (Guo et al., 2015; Pye et al., 2020). However, due to a low bias in simulated SO_4^{2-} mass concentration, the model underestimates aerosol acidity, resulting to a higher simulated pH value of approximately 2.0 during the summer period. In Europe, although the good agreement between our simulated pH and the result of Guo et al. (2018) (both are 3.9) supports the model simulations, we note the a significant overestimation of simulated alkaline species (sum of NH_4^+ and NH_3 , NMB = 17%) along with an underestimation of acidic species (sum of NO_3^- and HNO_3 , NMB = -57%; SO_4^{2-} , NMB = -51%) in December emphasizes the improvement of the aerosol. These discrepancies emphasize the need for improved representation of aerosol composition in the model. In northern China, the pH value calculated by Wang et al. (2016) was more than reported pH values that are about 2 units higher than our simulations (4.4 vs 6.7), and we suggest that the low bias is due Guo et al. (2017) found moderate acidic aerosol (pH = 5) during wintertime. We attribute this high bias in simulated pH to the underestimation of the cation mass

Formatted: English (United States)

Formatted: English (United States)

concentration of cations concentrations (e.g. Ca^{2+} , Mg^{2+}) in $\text{PM}_{2.5}$, as the mass concentrations of NH_4^+ , SO_4^{2-} , and NO_3^- are in the observational ranges of reported by Wang et al. (2016).

Formatted: Font color: Text 1

Table 7. Simulated pH value of $\text{PM}_{2.5}$ at single points certain locations compared with literature observational estimates of particle pH.

Location	Latitude	Longitude	Time Period	Method used	Field derived mean pH	Base	Meta	Reference
Egbert, ON, Canada	44.23	-79.78	Jul-Sep, 2012	E-AIM	2.1	3.77	1.57	Murphy et al. (2017)
Pasadena, CA, USA	34.14	-118.12	Jun, 2010	ISORROPIA	2.7	4.26	2.58	Guo et al. (2017)
Sao Paulo, Brazil	-23.55	-46.63	Aug-Sep, 2012	E-AIM	4.8	3.85	3.34	Vieira-Filho et al. (2016)
Cabauw, Netherland	51.97	4.93	Dec-Feb, 2012	ISORROPIA	3.9	3.91	3.58	Guo et al. (2018)
Xi'an, China	34.23	108.89	Nov-Dec, 2012	ISORROPIA	6.7	4.41	3.20	Wang et al. (2016)

Note: table extracted in part from Karydis et al. (2021).

5. Secondary inorganic aerosol composition

5.1 Size-resolved composition

The regional mass fractions of size-resolved inorganic aerosol components (NH_4^+ , SO_4^{2-} , and NO_3^-) are presented as bar charts in Figure 3, while global distribution maps of their size-resolved mass concentrations are shown in Figure S2, both the simulation results are derived from base case. To assess ammonia neutralization of sulfuric and nitric acids, we applied the chemical domain framework defined by Ge et al. (2022) based on SNA molar concentrations in PM_{10} with a threshold of $>1 \mu\text{g m}^{-3}$. The four chemical domains, illustrated in Figure 4, are defined as follows: “ SO_4^{2-} very rich” ($\text{totNH}_3/\text{totSO}_4 < 1$, totNH_3 : sum of NH_3 and NH_4^+ , totSO_4 : sum of SO_4^{2-} and HSO_4^-), “ SO_4^{2-} rich” ($\text{totNH}_3/\text{totSO}_4$ between 1 and 2), “ NO_3^- rich” (free $\text{NH}_3/\text{totNO}_3$ between 0 and 1, free NH_3 : totNH_3 minus double totSO_4 , totNO_3 : sum of NO_3^- and HNO_3), and “ NH_3 very rich” (free $\text{NH}_3/\text{totNO}_3 > 1$). Figure S3 shows the ratios used to define these domains.

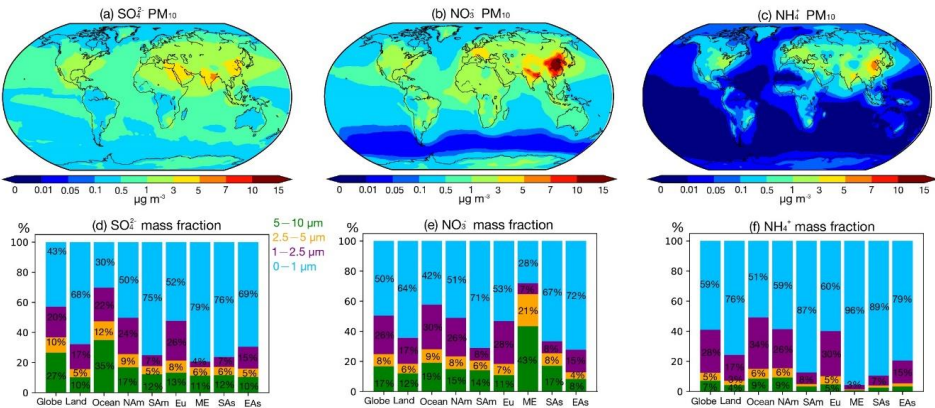


Figure 3. (a) – (c) global distribution of SO_4^{2-} , NO_3^- , and NH_4^+ mass concentration in the size range of $0 - 10 \mu\text{m}$, (d) – (f) bar plots for mean mass fractions of size-resolved NH_4^+ , SO_4^{2-} , and NO_3^- over globe, land, ocean and regions (marked in Figure 2), the size range of $5 - 10 \mu\text{m}$, $2.5 - 5 \mu\text{m}$, $1 - 2.5 \mu\text{m}$, and $0 - 1 \mu\text{m}$ are marked by green, orange, purple, and blue, respectively (NAM: North America; SAM: South America; Eu: Europe; ME: Middle East; SAs: South Asia; EAs: East Asia).

Regions with low inorganic aerosol concentrations ($< 1 \mu\text{g m}^{-3}$) are found in Southern Hemisphere oceans and remote areas such as the North Pole and South America, including the Amazon Basin. These areas represent relatively pristine baselines for evaluating anthropogenic impacts (Andreae et al., 1990; Andreae, 2007). In low northern latitude oceans, the “ SO_4^{2-} very rich” and “ SO_4^{2-} rich” domains dominate, characterized by NH_3 fully converted to NH_4^+ but incomplete neutralization of sulfuric acid where NH_3 is insufficient to fully neutralize sulfuric acid. As a result, sulfuric acid remains only partially neutralized, contributing to aerosol acidity. This pattern reflects low NH_3 emissions over oceans (Figure 1) and the contribution of biogenic dimethyl sulfide (DMS) to marine SO_4^{2-} (Fiddes et al., 2018; Jackson et al., 2020). Additional NO_x and SO_2 from shipping contribute to marine SO_4^{2-} and NO_3^- (Wang et al., 2023; Burgard and Briä, 2016). Average PM_{10} SNA concentrations are lower over oceans compared to land (NH_4^+ : $0.06 \mu\text{g m}^{-3}$ vs. $0.36 \mu\text{g m}^{-3}$; NO_3^- : $0.37 \mu\text{g m}^{-3}$ vs. $1.24 \mu\text{g m}^{-3}$; SO_4^{2-} : $0.60 \mu\text{g m}^{-3}$ vs. $0.95 \mu\text{g m}^{-3}$). Marine SO_4^{2-} and NO_3^- are predominantly in the super-micron mode, with mass fractions of 70% and 58%, respectively. Coastal areas exhibit a “ NO_3^- rich” domain due to continental outflows (Figure S2S3) (Prospero et al., 1985), consistent with prior findings that marine aerosol in the super-micron mode primarily comprises inorganic salts, including sea salt, non-sea salt sulfate, and nitrate, while organic matter is concentrated in the sub-micron range (Russell et al., 2023; Cavalli et al., 2004).

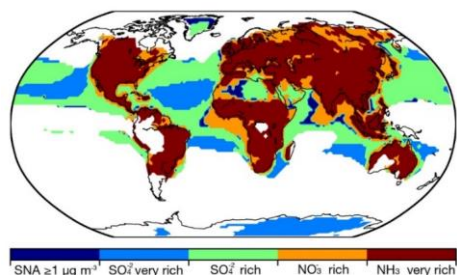


Figure 4. Distribution of ammonia neutralization state of sulfuric and nitric acids, based on SNA molar concentrations in PM_{10} with a threshold of $\geq 1 \mu\text{g m}^{-3}$, where the SNA mass concentration less than the threshold is measured by blank zone. The “ SO_4^{2-} very rich” represents the ratio of totNH_3 to totSO_4 less than 1 (totNH_3 : sum of NH_3 and NH_4^+ , totSO_4 : sum of SO_4^{2-} and HSO_4^-), the “ SO_4^{2-} rich” represents the ratio of totNH_3 to totSO_4^{2-} between 1 and 2, the “ NO_3^- rich” represents the ratio of free NH_3 to totNO_3 between 0 and 1 (free NH_3 : totNH_3 minus double totSO_4 , totNO_3 : sum of NO_3^- and HNO_3), and the “ NH_3 very rich” represents the ratio of the free NH_3 to totNO_3 over 1.

On land, except for areas such as northern Russia, central Africa, and the Arabian Peninsula, the aerosol typically falls within the “ NH_3 very rich” domain. In this domain, SO_4^{2-} is fully-neutralized by the available NH_3 , with sufficient NH_3 available remaining to additionally-neutralize NO_3^- , making. As a result, NO_3^- becomes the limiting factor in NH_4NO_3 the formation of NH_4NO_3 . More than 60% of SNA mass is in the sub-micron mode on land, while the super-micron modes (i.e. $1 - 2.5 \mu\text{m}$, $2.5 - 5 \mu\text{m}$ and $5 - 10 \mu\text{m}$) accounts for a smaller fraction (7% for NH_4^+ , 15% for

865 SO_4^{2-} , and 18% for NO_3^-). In polluted regions such as East and South Asia, PM_{10} SNA concentrations are three times
higher than the global land average. For example, East Asia shows NH_4^+ : $1.88 \mu\text{g m}^{-3}$, NO_3^- : $5.31 \mu\text{g m}^{-3}$, and SO_4^{2-} :
2.29 $\mu\text{g m}^{-3}$, while South Asia records NH_4^+ : $1.58 \mu\text{g m}^{-3}$, NO_3^- : $3.68 \mu\text{g m}^{-3}$, and SO_4^{2-} : $3.18 \mu\text{g m}^{-3}$. Free NH_3 is
abundant in regions like southern North America, Europe, South Asia, and East Asia, with mean free NH_3 /total NO_3^-
870 ratios of 2.11, 3.77, 5.30, and 3.78, respectively. Over 75% of SNA mass in these regions is concentrated in the 0–
1 μm and 1–2.5 μm size ranges. The NH_3 surplus reflects recent trends in precursor emissions, with stable or
increasing NH_3 emissions contrasting with declining SO_2 and NO_x emissions (Zheng et al., 2018; Hand et al., 2012;
Russell et al., 2012). In the Middle East, particularly the Arabian Peninsula, aerosol is dominated by desert dust with
negligible NH_3 emissions. The “ SO_4^{2-} rich” and “ NO_3^- rich” domains predominate, where insufficient NH_3 levels are
insufficient to neutralize acidic components fully, limiting NH_4NO_3 formation. Mean concentrations of NH_4^+ , NO_3^- ,
875 and SO_4^{2-} in this region are $0.72 \mu\text{g m}^{-3}$, $2.07 \mu\text{g m}^{-3}$, and $3.19 \mu\text{g m}^{-3}$, respectively. Over 70% of NO_3^- resides in the
super-micron modes due to interactions with sea salt and crustal dust, which shift NO_3^- from sub-micron to super-
micron modes (Chen et al., 2020; Koçak et al., 2007; Karydis et al., 2016). Sub-micron NH_4^+ and SO_4^{2-} remain
dominant, accounting for 96% and 79% of their respective fractions, consistent with Osipov et al. (2022), who
identified anthropogenic sources as the primary contributors to fine particles in the region.

Formatted: Highlight

880 5.2 NH_3 column concentration

Figure 5-(a)5a shows the global distribution of NH_3 column concentration. The global area-weight mean value of
 NH_3 column concentration is 0.80 mg m^{-2} , with the highest value up to 30 mg m^{-2} in the Indo-Gangetic Plain of India
and the lowest value of less than 0.01 mg m^{-2} in the remote oceans of the Southern Hemisphere and the South Pole.
Compared with previous studies that investigated NH_3 column concentrations based on satellite retrievals (Van
885 Damme et al., 2014; Van Damme et al., 2015; Zhou et al., 2024), our results can capture the distribution of NH_3
hotspots worldwide, including the Indo-Gangetic Plain, the North China Plain, and West Africa and Amazonia, where
biomass burning is dominant (Van Damme et al., 2018). However, Van Damme et al. (2018) pointed out that two-
thirds of the NH_3 emission hotspots are underestimated by at least one order of magnitude in the NH_3 emission
inventory EDGAR (CAMSGLOBANT used in this study is derived from EDGAR, see 2.1.1). Given such an
890 underestimation in the current NH_3 emission inventory, we further improve the emission by applying a new inventory
and updating the current inventory using a top-down method introduced in Section 2.1. The simulation results are
discussed in Section 7.

Formatted: Font: Times New Roman, 10 pt, English
(United States)

Formatted: Indent: First line: 0.51 cm, Line spacing: 1.5
lines, Widow/Orphan control, Don't adjust space
between Latin and Asian text, Don't adjust space
between Asian text and numbers

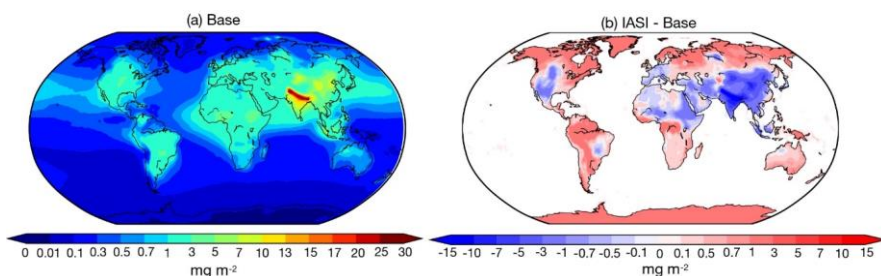


Figure 5. Global distribution of (a) the average NH_3 column concentration (mg m^{-2}) for the Base Case, and (b) the absolute difference between IASI satellite retrieval and Base case, from 2010 to 2012.

Our simulated NH_3 column concentrations show good agreement with the IASI satellite observations (Figure 5b), with global land mean values at a comparable level of 1.66 mg m^{-2} . However, regional biases can be significant, with an NMB of -0.32 . The model overestimates NH_3 column concentrations over regions such as India, China, western America, and northeastern Africa, while it has a negative bias in high-latitude regions. It is also important to note that biases in the IASI satellite products have been identified in previous studies (Dammers et al., 2017; Dammers et al., 2019), more details are discussed in Section 2.1.2.

5.3 Global NH_3 budget

The global budget for NH_3 and NH_4^+ is summarized in Table 8. Given a global NH_3 emission input of $74.3773.3 \text{ Tg yr}^{-1}$, the global burden and lifetime derived from the base case simulation are 0.414 Tg and 2.040 days, respectively; for NH_4^+ , the global burden and lifetime are 0.343 Tg and 3.461 days, respectively. Based on the simulations of nine models, Bian et al. (2017) assessed that given the average NH_3 emission input of $76.384 \text{ Tg yr}^{-1}$, the average global burden and lifetime for NH_3 and NH_4^+ are 0.292 Tg and 0.727 days, and 0.323 Tg and 4.3 days, respectively. Compared to Bian et al. (2017), our study uses the same NH_3 emission input; however, the global burden and lifetime of NH_3 derived from the base case are larger. This potential overestimation may be attributed to the wet deposition scheme used in EMAC. The scavenging scheme (SCAV) accounts for pH adjustments in NH_3 dissolution. More specifically, the EMAC model implicitly determines the effective Henry's law constant by solving a system of coupled ordinary differential equations, explicitly representing liquid-phase processes in clouds and raindrops, including dissociation, acid-base equilibria, redox reactions, and photolysis (Tost et al., 2006). This approach ensures a comprehensive calculation of total wet deposition for NH_4^+ and NH_3 . Notably, the NH_3 burdens simulated in the AeroCom model intercomparison by Bian et al. (2017) exhibit significant variability, spanning a factor of 17. This wide range underscores the sensitivity of atmospheric NH_4^+ and NH_3 burdens and lifetimes to model domain definitions, deposition pathways, and NH_3 chemical processes across different models (Ge et al., 2022).

Table 8. Atmospheric budget of NH_3 , NH_4^+ , and NH_x ($\text{NH}_3 + \text{NH}_4^+$).

Simulation Case	Specie	Emission (Tg yr^{-1})	Burden (Tg)	Dry Deposition (Tg yr^{-1})	Wet Deposition (Tg yr^{-1})	Lifetime ^a (day)
Base	NH_3	73.273	0.414	28.222	-	2.040
CEDS		77.131	0.434	29.909	-	2.041.9
Top-Dep		84.717	0.414	34.364	-	1.777

Base		-	0.343	1.162	34.697	3.461
CEDS	NH ₄ ⁺	-	0.354	1.253	35.778	3.459
Top-Dep		-	0.353	1.525	36.192	3.392.9
Base		-	0.757	29.384	34.697	3.685
						(4.270) ^b
CEDS	NH _x	-	0.788	31.452	35.778	3.668
						(4.254)
Top-Dep		-	0.767	35.909	36.212	3.270
						(3.855)

^a: NH₃ lifetime = Burden/Emission; NH₄⁺ lifetime = Burden/(Dry Deposition + Wet Deposition);

^b: NH_x lifetime = NH_x Burden/ NH₃ Emission; in the parentheses, NH_x lifetime = NH_x Burden/ (Dry Deposition + Wet Deposition);

Considering the SCAV scavenging scheme, we further calculate the global budget for NH_x (NH₃ + NH₄⁺) in Table 8. The global burden of NH_x is 0.757 Tg. Wet and dry deposition contribute almost equally to the sink accounting for 54% and 46%, respectively. The lifetime of NH_x is 3.685 – 4.270 days, depending on the calculation method. Ge et al. (2022) estimated a global budget for NH_x, with an input NH₃ emission of 64.485 Tg yr⁻¹. They calculated the global burden of NH_x to be 0.949 Tg, with a lifetime of 4.9–5.2 days and its wet and dry deposition contributing equally to the sink (i.e., 51% and 49% of total deposition, respectively).

6. Aerosol acidity

Figure 6 illustrates the global distributions of size-resolved aerosol pH, with regional averages summarized in Table 9. Aerosol pH exhibits marked spatial variations, influenced by land-sea contrasts and regional sources. Over land in the Northern Hemisphere, excluding deserts, aerosols are generally acidic, whereas marine aerosols are alkaline due to sea salt influence. However, high-latitude marine aerosols are generally more acidic than those over remote ocean regions, primarily due to the low liquid water content/long-range transport of anthropogenic pollutants such as H₂SO₄ and hydrogen ion outflow/HNO₃ from land-continental sources (Myhre et al., 2013; Karydis et al., 2021). The average pH values for land-based aerosols are 4.2 (5–10 μm), 4.2 (2.5–5 μm), 3.9 (1–2.5 μm), and 4.3 (0–1 μm). In contrast, marine aerosol pH values are 6.2 (5–10 μm), 5.8 (2.5–5 μm), 5.1 (1–2.5 μm), and 5.1 (0–1 μm). The deserts of North Africa, the Middle East, and the Gobi maintain the highest pH values (>7) across all size ranges, driven by non-volatile cations (e.g., Ca²⁺, Mg²⁺) that neutralize acidic components and enhance water uptake.

Regionally, higher pH values (5–5.7) in the Middle East are attributed to airborne dust, while coastal areas like the western Arabian Gulf have lower aerosol pH (<3 in 0–1 μm) due to elevated sulfate concentrations. In South Asia, abundant NH₃ emissions keep pH values between 5.4 and 4.9 despite high SO₂ and NO_x emissions. East Asia shows a distinct pH gradient, with desert regions in the northwest reaching pH >7 across all sizes, and southeast coastal areas exhibiting low pH (2–4), linked to significant SO₂ emissions and sulfate formation. Europe (pH 3.7–4.1) and North America (pH 3.2–3.6) demonstrate moderate acidity, with the western USA exhibiting higher values (4–6) due to desert influences. In South America, pH ranges from 3.9 to 4.5, with coastal regions exceeding 6 due to sea salt.

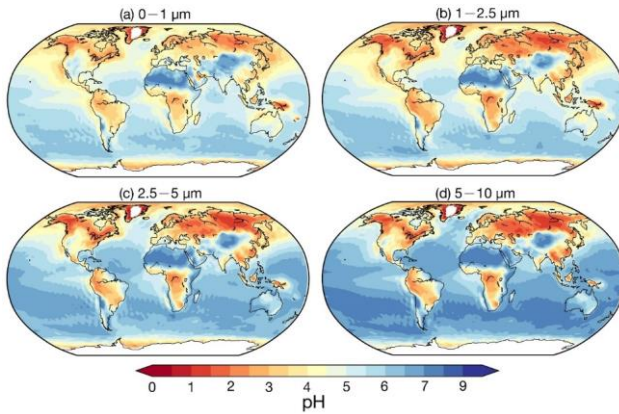


Figure 6. Global distribution of surface average aerosol pH values in the size ranges: (a) 0 – 1 μm , (b) 1 – 2.5 μm , (c) 2.5 – 5 μm , (d) 5 – 10 μm , derived from Base case from 2010 to 2012.

An increasing trend in pH is observed from North America to Europe and East Asia, consistent with prior studies (Zhang et al., 2021a; Ding et al., 2019; Guo et al., 2017a). Aerosol alkalinity is driven by NH_4^+ and non-volatile cations, which neutralize SO_4^{2-} and NO_3^- , while water-soluble ions (WSIs) enhance liquid water uptake. East Asia exhibits the highest pH among regions, facilitated by relatively lower SO_4^{2-} , abundant NH_4^+ and WSIs, and significant NO_3^- and non-volatile cations in the coarse modes. These chemical properties outweigh the influence of meteorological effects such as differences in temperature and humidity.

Table 9. Size-resolved pH values across the globe and regions from simulation cases.

Region	0 – 1 μm			1 – 2.5 μm			2.5 – 5 μm			5 – 10 μm		
	Base ^a	Meta ^a	noNH ₃ ^a	Base ^a	Meta ^a	noNH ₃ ^a	Base ^a	Meta ^a	noNH ₃ ^a	Base ^a	Meta ^a	noNH ₃ ^a
Globe	4.9	4.19	3.28	4.83	4.3	4.09	5.38	5	4.82	5.75	5.47	5.46
Land	4.29	2.96	1.06	3.94	2.9	1.71	4.19	3.36	2.51	4.23	3.54	3.11
Ocean	5.1	4.58	3.99	5.11	4.75	4.86	5.76	5.52	5.56	6.24	6.08	6.21
North America	3.62	2.63	1.01	3.16	2.38	1.17	3.31	2.63	1.83	3.38	2.81	2.34
South America	4.11	3.25	1.46	3.85	3.26	2.26	4.4	4	3.25	4.52	4.22	3.84
Europe	4.09	2.97	0.84	3.65	2.8	1.27	3.69	2.92	1.91	3.75	3.08	2.67
Middle East	5.02	1.94	-0.17	5.25	2.08	0.51	5.47	3.59	1.86	5.66	4.18	3.85
South Asia	5.42	2.8	-0.2	4.86	2.33	0.43	5	2.73	1.37	5.04	2.88	2.16
East Asia	5.15	3.23	0.5	4.65	3.32	1.16	4.56	3.24	1.76	4.54	3.26	2.3

^a: average pH value.

Contrary to previous findings (e.g. Kakavas et al., 2021; Ding et al., 2019), which suggest decreasing aerosol acidity with increasing particle size, pH in the base case (stable state) for 0–1 μm exceeds that of 1–2.5 μm over many regions, excluding oceans and the Middle East. This is examined through three perspectives. First, the assumption of phase state. As described in Section 2.2.1, the pH predictions based on the metastable state tend to be lower than those based on the stable state under low RH conditions. Although previous studies concluded that the

Formatted: Indent: First line: 0.51 cm, No widow/orphan control, Adjust space between Latin and Asian text, Adjust space between Asian text and numbers, Tab stops: Not at 1.27 cm

choice between stable and metastable assumption in ISORROPIA has no significant impact on pH predictions (Song et al., 2018), our sensitivity simulation (Meta case) assuming metastable conditions revealed (Meta case) yields consistently lower pH values across all sizes, with the greatest particle size ranges. The differences in pH relative to the base case are shown in Figure 7 and Table 9. The most substantial reductions are observed in regions with high mineral cations and/or low relative humidity (RH), such as South Asia and the Middle East. In the metastable state, all anions remain aqueous, resulting in, where the pH decreases by more acidic aerosols than 2 units. These results are consistent with the findings of Karydis et al. (2021) and Milousis et al. (2024). For instance, Karydis et al. (2021) reported that the stable-state assumption yields global average pH values approximately 0.5 units higher than those from the metastable assumption, comparable to the magnitude of differences calculated in our study (Table 9).

While the Meta case explains some discrepancies, pH in the 0–1 μm size range remains higher relative to the 1–2.5 μm range in several regions (Table 5). Another sensitivity simulation, removing $\text{NH}_3/\text{NH}_4^+$ emissions (no NH_3 case), significantly reduced pH across all sizes over land, especially in NH_3 -rich regions like South Asia and the Middle East, where 0–1 μm pH dropped below zero. This indicates increased pH sensitivity in the fine size ranges (i.e., 0–1 μm and 1–2.5 μm), particularly in regions where NH_3 availability is abundant. Excluding NH_3 , results in a consistent pH increase with particle size across all regions. Finally, as discussed in Section 4.1, the comparison with observed size-resolved mass concentrations from the EMEP network revealed and $\text{NH}_3/\text{NH}_4^+$ partitioning ratio reveals an underestimation of acidic components (SO_4^{2-} and NO_3^-) and an overestimation of alkaline components in the 0–1 μm size range. This, along with an inadequate treatment of $\text{NH}_3/\text{NH}_4^+$ partitioning. This chemical imbalance contributes to the anomalously high simulated pH in the fine mode (0–1 μm). For instance, the observed SO_4^{2-} , NO_3^- and NH_4^+ in 0–1 μm accounts for 91%, 59% and 67% of 0–2.5 μm at the Montseny site (41.78° N, 2.35° E) during 2010–2012 (observed NH_4^+ only available in 2010), respectively, compared to the accounting of 79%, 54% and 77% in simulation, highlighting a need for improved representation of aerosol composition in fine modes. In addition, the observed mean NH_4^+ partitioning ratios ($\text{NH}_4^+ / (\text{NH}_3 + \text{NH}_4^+)$, in $\mu\text{mole m}^{-3}$) during 2010–2012 from EMEP, NNDMN, and AMoN networks are 49%, 49%, and 50%, respectively. Our model shows low biases, with the mean ratios of 32%, 39%, and 41%. These results reinforce the necessity of refining the treatment of $\text{NH}_3/\text{NH}_4^+$ partitioning to better capture the size-resolved trend of aerosol acidity.

This study calculates Part of the discrepancy in size-resolved aerosol pH based on a log-normal calculations between models may arise from differences in how particle size distributions and gas-particle partitioning are treated. EMAC model uses a lognormal size distribution, differing from other approaches. For instance, and applies ISORROPIA separately to each size mode to calculate gas-aerosol partitioning. In contrast, other studies (e.g., Kakavas et al., 2021) used the PMCAMx model, which employs a employ sectional approach to track approaches, where gas-aerosol mass and composition across 10 size bins ranging from 40 nm to 40 μm . The partitioning is first five bins represent performed on the PM_{10} fraction (0.04–1.25 μm), while three bins cover sizes up bulk aerosol phase, and the resulting condensed mass is then distributed across size bins based on the available surface area. These fundamental differences in modeling assumptions can lead to 40 μm . In addition variations in the predicted distribution of aerosol components across size ranges, which in turn affects the calculated size-resolved pH. Moreover, previous studies on investigating size-resolved aerosol acidity also have certain limitations. For example instance, a laboratory

Formatted: Font color: Auto

Formatted: Font color: Auto

Formatted: Font color: Auto, English (United Kingdom)

Formatted: Font color: Auto, English (United Kingdom)

Formatted: English (United Kingdom)

study observed increasing aerosol acidity with decreasing particle size, but this trend only holds for pH below 2 (Craig et al., 2018). Similarly, a field study [reached by Fang et al. \(2017\)](#) reported the same [conclusion trend](#) but lacked [concurrent](#) measurements of key gas-phase species ([Fang et al., 2017](#)), which limits the interpretability of the results.

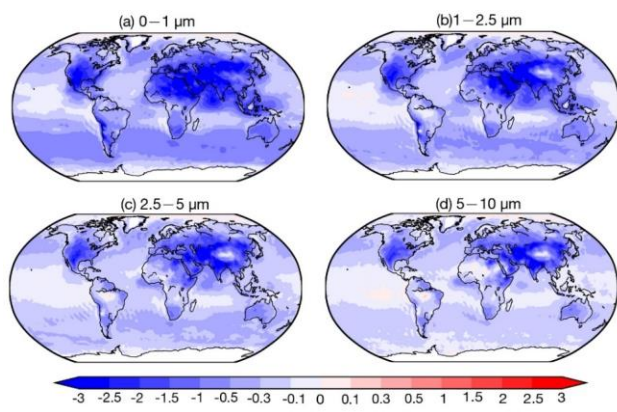


Figure 7. Global distribution maps of pH value absolute difference between Meta case and base case in the size ranges of 0 – 1 μm , 1–2.5 μm , 2.5–5 μm , and 5 – 10 μm , averaged from 2010 to 2012.

7. Emission Sensitivity Analysis

The formation of secondary inorganic aerosols is strongly linked to NH_3 emissions (Wu et al., 2016; Chen et al., 2019; Liang et al., 2024). Xu et al. (2020) and Wang et al. (2015) have highlighted the critical role of gas-particle partitioning of $\text{NH}_3/\text{NH}_4^+$ in SNA formation, which is influenced by factors such as temperature, aerosol water content, and aerosol acidity (Nenes et al., 2020). Notably, the $\text{NH}_3/\text{NH}_4^+$ partitioning process buffers aerosol acidity, maintaining stability even amid shifts in acidic species like NO_3^- and SO_4^{2-} (Karydis et al., 2021). These findings suggest that the effects of NH_3 emissions on SNA formation and aerosol acidity remain [a subject of debate/understudied](#) (Weber et al., 2016; Zheng et al., 2022; Fu et al., 2017; Zou et al., 2024). However, most studies have focused on fine particles ($\text{PM}_{2.5}$ or PM_{10}), polluted regions (e.g., northern China), and haze episodes (Ge et al., 2019; Gao et al., 2016). Modeling studies often evaluate the effects of NH_3 emission changes by uniformly altering emission levels within each grid (Pozzer et al., 2017; Fu et al., 2017). While such approaches provide valuable insights, they may lack feasibility as NH_3 abundance correlates with population density, making uniform changes less representative of real-world scenarios. To address this, we compare the effects of two NH_3 emission schemes CEDS and Top-Dep on size-resolved SNA mass concentration and aerosol acidity relative to [the](#) base case.

The NH_3 mass concentration serves as a proxy for NH_3 emissions, and differences in NH_3 mass concentrations between the scenarios and the base case (Figure [S6S4](#)) align with corresponding emission differences (Figure 1). Figures [78](#) and [89](#) show the responses of size-resolved NH_4^+ , NO_3^- , and SO_4^{2-} mass concentrations to NH_3 emission changes in the CEDS and Top-Dep cases, respectively. Similarly, Figure [910](#) illustrates the size-resolved aerosol acidity responses for the two cases. Additional details are provided in supplementary figures: Figures [S5](#) – [S7](#)–[S9](#)

(CEDS case) and Figures S44–S43S8–S10 (Top-Dep case) depict the size-resolved responses of NH_4^+ , NO_3^- , and SO_4^{2-} mass concentrations, while Figures S40S11 and S44S12 highlight changes in size-resolved aerosol acidity.

The regional gas-particle partitioning ratios for $\text{NH}_3/\text{NH}_4^+$ ($\epsilon(\text{NH}_4^+) = \text{NH}_4^+ / (\text{NH}_4^+ + \text{NH}_3)$) and $\text{NO}_3^-/\text{HNO}_3$ ($\epsilon(\text{NO}_3^-) = \text{NO}_3^- / (\text{NO}_3^- + \text{HNO}_3)$) are shown in Figure S45S13. Regional emission amounts of NO_x and SO_2 from the CAMS and CEDS_GBD inventories are detailed in Table S1.

7.1 Size-Resolved SNA Response

Regarding the atmospheric budget of NH_3 (Table 8), a modest increase in global NH_3 emissions (CEDS case) slightly raises the deposition of NH_3 and shortens the lifetime. Meanwhile, both the burden and deposition of NH_3 and NH_4^+ , while the are increased, with a longer lifetime remains unchanged. In contrast, the larger emission increase in the Top-Dep cases does not alter the $\text{NH}_3/\text{NH}_4^+$ burden but leads to higher deposition and a shorter lifetime for both species.

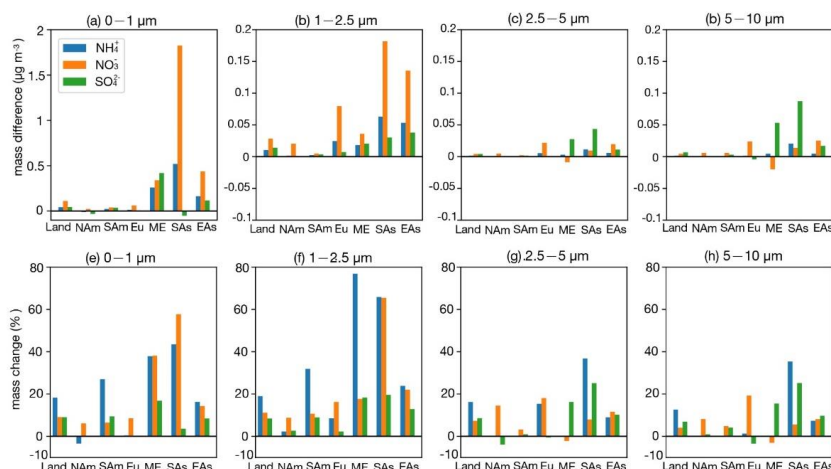


Figure 78. Bar plots for regional surface SNA mass concentration ($\mu\text{g m}^{-3}$) absolute difference between CEDS case and base case in the four size ranges (a)–(d); change ratio in the four size ranges (e)–(h). The calculation of change ratio in the size range of 0–1 μm is based on the mask of 0.1 $\mu\text{g m}^{-3}$, the change ratio in the size range of 1–2.5 μm , 2.5–5 μm and 5–10 μm is based on the mask of 0.05 $\mu\text{g m}^{-3}$ (Land: global land; NAm: North America; SAm: South America; Eu: Europe; ME: Middle East; SAs: South Asia; EAs: East Asia).

Across land regions, a small increase in NH_3 emissions (CEDS case), along with rising NO_x and SO_2 emissions, slightly raises $\epsilon(\text{NH}_4^+)$ while marginally lowering $\epsilon(\text{NO}_3^-)$ (Figure S45S13). The SNA mass concentration increases consistently across size ranges, with the most notable growth in NH_4^+ and NO_3^- in the 1–2.5 μm range (19% and 11%, respectively) and SO_4^{2-} in the submicron particles (9%). Under a larger NH_3 emission increase (Top-Dep case), $\epsilon(\text{NH}_4^+)$ drops significantly, and $\epsilon(\text{NO}_3^-)$ decreases slightly. The SNA response becomes more pronounced, with substantial increases in the 1–2.5 μm range (NH_4^+ : 104%, NO_3^- : 41%, SO_4^{2-} : 23%), while NO_3^- and SO_4^{2-} decrease

Formatted: Font: Italic

Formatted: Font: Italic

Formatted: Indent: First line: 0.51 cm, Line spacing: 1.5 lines

Formatted: Font color: Text 1

Formatted: Font color: Text 1

Formatted: Font color: Text 1

Formatted: Font color: Text 1

Formatted: Font color: Text 1

Formatted: Font color: Text 1

Formatted: Font color: Text 1

Formatted: Font: Italic

Formatted: Font: Italic

Formatted: Font: Italic

Formatted: Font: Italic

in coarser particles. These shifts are linked to higher NH_3 emissions in relatively clean, high-latitude regions with low NH_3 flux (Figure 1c), which elevate NH_3 concentrations (Figure S6S4) enhancing NH_4^+ formation (Figure S4+S8).

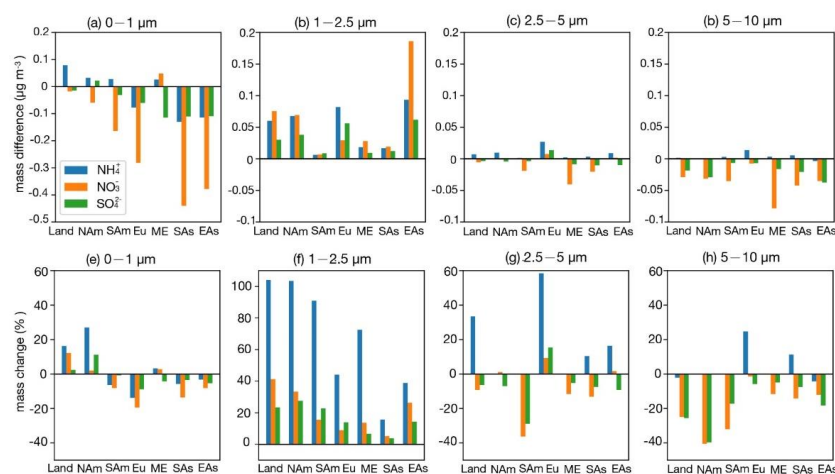


Figure 8. Bar plots for regional surface SNA mass concentration ($\mu\text{g m}^{-3}$) absolute difference between Top-Dep case and base case in the four size ranges (a)–(d); change ratio in the four size ranges (e)–(h). The calculation of change ratio in the size range of 0–1 μm is based on the mask of $0.1 \mu\text{g m}^{-3}$, the change ratio in the size range of 1–2.5 μm , 2.5–5 μm and 5–10 μm is based on the mask of $0.05 \mu\text{g m}^{-3}$ (Land: global land; NAm: North America; SAm: South America; Eu: Europe; ME: Middle East; SAs: South Asia; EAs: East Asia).

Regional analysis of SNA responses in Europe shows that a 23% reduction in NH_3 emissions, along with increases in NO_x and SO_2 emissions (CEDs case), raises $\hat{c}(\text{NH}_4^+)$ slightly while causing a minor drop in $\hat{c}(\text{NO}_3^-)$. The SNA mass increases mainly in the 1–2.5 μm range, with a slight decrease in SO_4^{2-} in coarser particles. Since Europe has abundant NH_3 , reductions are offset by existing availability and rising NO_x and SO_2 levels, leading to additional NH_4NO_3 and $(\text{NH}_4)_2\text{SO}_4$ formation. With higher NH_3 emissions (Top-Dep-Top-Dep case), the response becomes more complex: SNA decreases in the submicron particles (Figure 8e9e) but increases in larger particles (Figure 8f9f–g), with the largest growth seen in NH_4^+ (~50%).

Formatted: Font: Italic

Formatted: Font: Italic

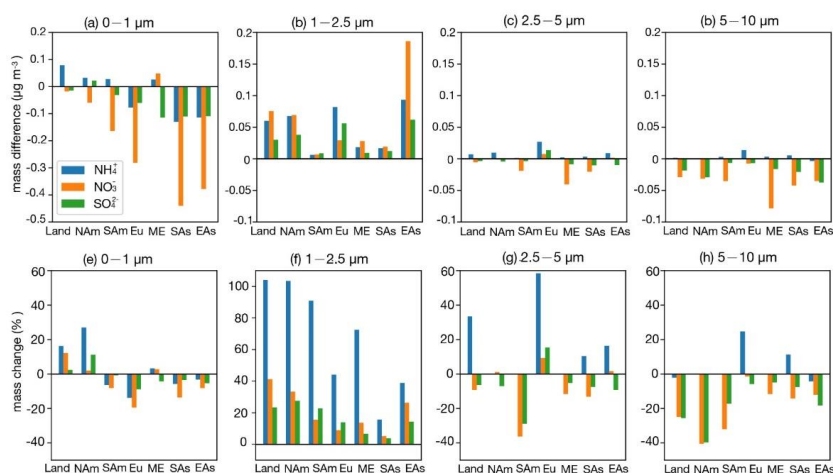


Figure 9. The same as Figure 8, but for the difference between Top-Dep case and base case.

In East Asia, reducing NH_3 emissions while increasing NO_x and SO_2 emissions (CEDS case) raises $\epsilon(\text{NH}_4^+)$ and slightly increases $\epsilon(\text{NO}_3^-)$. SNA grows across all particle sizes, with the most significant changes in 1–2.5 μm range (Figure 7a8f). A similar NH_3 reduction in the Top-Dep case produces comparable $\epsilon(\text{NH}_4^+)$ and $\epsilon(\text{NO}_3^-)$ changes, with SNA mainly decreasing in the submicron particles. The response in East Asia resembles that of Europe, where abundant NH_3 buffers SNA changes. In South Asia, NH_3 and NO_x emissions rise in the CEDS case while SO_2 emissions decline, slightly lowering $\epsilon(\text{NH}_4^+)$ and increasing $\epsilon(\text{NO}_3^-)$. NH_4^+ and NO_3^- concentrations grow across all size ranges (Figure 8), with the largest NH_4^+ increase found in 1–2.5 μm particles (66%) and NO_3^- rising in both submicron and 1–2.5 μm particles (~60%). SO_4^{2-} decreases in submicron particles but increases in coarser ones (25%). Conversely, reducing NH_3 emissions in the Top-Dep case raises $\epsilon(\text{NH}_4^+)$ and lowers $\epsilon(\text{NO}_3^-)$, leading to SNA declines, especially in submicron particles. South Asia, with abundant NH_3 , shows NO_3^- as the limiting factor for NH_4NO_3 formation, driving strong $\epsilon(\text{NO}_3^-)$ and NO_3^- responses in finer particles.

In North America, NH_3 and SO_2 emissions decrease, while NO_x emissions slightly rise (CEDS case). $\epsilon(\text{NH}_4^+)$ increases marginally, whereas $\epsilon(\text{NO}_3^-)$ declines slightly. NH_4^+ and SO_4^{2-} show minor reductions in submicron particles, while NO_3^- increases. In the Top-Dep case, a sharp rise in NH_3 emissions, mainly over Canada and Greenland, significantly lowers $\epsilon(\text{NH}_4^+)$, stabilizes $\epsilon(\text{NO}_3^-)$, and increases NH_4^+ and SO_4^{2-} in 1–2.5 μm particles. In South America, a small NH_3 emission rise (CEDS case) has little effect on $\epsilon(\text{NH}_4^+)$ or $\epsilon(\text{NO}_3^-)$, resulting in minimal aerosol composition changes. However, a substantial NH_3 increase (Top-Dep case) significantly boosts NH_3 concentrations, reduces $\epsilon(\text{NH}_4^+)$ and $\epsilon(\text{NO}_3^-)$, and shifts aerosol partitioning to smaller particles, particularly in central regions. Decreased NO_3^- and SO_4^{2-} in surrounding areas (Figures 842–43S9–10) suggest NH_3 is neutralizing transported species, explaining the observed $\epsilon(\text{NO}_3^-)$ reduction. Changes in other particle size ranges are minimal. In the Middle East, NH_3 emissions rise moderately (20%), along with slight NO_x and SO_2 increases (CEDS case). $\epsilon(\text{NH}_4^+)$ and $\epsilon(\text{NO}_3^-)$ remain stable, with NH_4^+ and NO_3^- increasing mainly in submicron particles (~40%), while SO_4^{2-} grows across

Formatted: Font: Italic

Formatted: Font: Italic

Formatted: Font: Italic

Formatted: Font: Italic

Formatted: Font: Italic

Formatted: Font: Italic

Formatted: Font: Italic

Formatted: Font: Italic

Formatted: Font: Italic

Formatted: Font: Italic

Formatted: Font: Italic

Formatted: Font: Italic

Formatted: Font: Italic

Formatted: Font: Italic

Formatted: Font: Italic

Formatted: Font: Italic

Formatted: Font: Italic

Formatted: Font: Italic

Formatted: Font: Italic

sizes (~15%). A minor NH₃ emission drop (Top-Dep case) reduces NH₃ concentrations but enhances SNA in 1–2.5 μm particles, highlighting compensatory NH₃ effects in "NH₃ very rich" domains.

Overall, higher NH₃ emissions enhance SNA formation, particularly in the fine size ranges (0–1 μm and 1–2.5 μm). Greater NH₄⁺ formation (e.g., Top-Dep case) depletes NO₃⁻ and SO₄²⁻ from coarse size ranges, leading to decreases in 2.5–5 μm and 5–10 μm. In low-SNA regions (e.g., South America, Greenland), NH₃ increases have limited SNA impacts but substantially elevate NH₃ concentrations. In "NH₃ very rich" regions (e.g., East Asia, Europe), NH₃ reductions alone may still increase $\delta(\text{NH}_4^+)$, promoting further SNA formation. These findings align with Zou et al. (2024), emphasizing the greater effectiveness of NO_x reductions in PM_{2.5} mitigation compared to NH₃ or SO₂ control in ammonia-rich environments. Coordinated control of precursor emissions is crucial for mitigating air pollution, especially in heavily polluted regions (Wen et al., 2024).

7.2 Aerosol acidity response

7.2.1 Size-resolved pH changes

Among atmospheric buffering agents (e.g., conjugate acid-base pairs like NH₃/NH₄⁺ and CO₂/HCO₃⁻, as well as organic acids), the NH₃/NH₄⁺ acid-base pair exhibits the largest buffering capacity for aerosols, dominating much of the continental urban areas (Zheng et al., 2023; Zheng et al., 2020). When NH₃ emissions are entirely eliminated, changes in [oceanic aerosol](#) pH values are negligible compared to the base case (noNH₃ case, Table S9 and Figure S5S14). However, aerosols over land become significantly more acidic, with pH values in the 0–1 μm size range dropping to -0.2 in South Asia and -0.17 in the Middle East. (Figure 10). The most substantial pH decreases occur in 0–1 μm aerosols, primarily in South Asia, East Asia, Europe, North America, and South America, consistent with the "NH₃-buffered regions" identified by Zheng et al. (2020).

Interestingly, while neither the Middle East nor northern Africa are categorized as "NH₃-buffered regions," noticeable pH decreases are observed in the 0–1 μm and 1–2.5 μm size ranges over the Middle East, including Egypt and Libya. In these regions, the SNA is dominated by "SO₄²⁻ rich" and "NO₃⁻ rich" chemical domains (Figure 4), where NH₄⁺ cannot fully insufficient NH₃ levels are to neutralize the acidic components, resulting in available NO₃⁻ and SO₄²⁻. This results in excess acidic components, particularly in the 0–1 μm and 1–2.5 μm size ranges (Figure S2S3). Without NH₃ emissions, the abundance of NO₃⁻ and SO₄²⁻ further increases aerosol acidity.

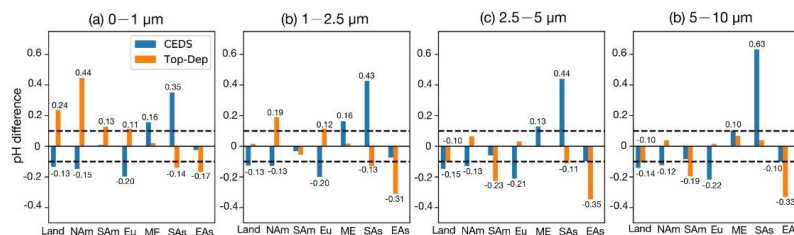


Figure 910. Bar plots for pH value absolute difference between CEDS/Top-Dep case and base case in the four size ranges (a) – (d), with the two dashed lines representing the value of 0.1 and -0.1, respectively (Land: global land; NAm: North America; SAm: South America; Eu: Europe; ME: Middle East; SAs: South Asia; EAs: East Asia).

Compared to the base case, size-resolved pH values in the CEDS case show an average decrease of -0.13 to -0.15 units over land. The most pronounced decreases occur in remote regions of the Northern Hemisphere (Figure S40S11), where NH_3 emission flux is relatively low. In contrast, the Top-Dep case exhibits an average pH increase of 0.24 units in the 0–1 μm range over land, driven by the higher NH_3 emission flux. This NH_3 -driven alkalization effect is less pronounced in the 1–2.5 μm range due to counteracting acidification effects from newly formed acidic components, as suggested by Zheng et al. (2024). Notably, pH decreases of -0.10 units are found in the 2.5–5 μm and 5–10 μm size ranges.

In East Asia, the pH changes in the CEDS case are concentrated in the 2.5–5 μm and 5–10 μm ranges (-0.10 units in both), with minimal changes in 0–1 μm and 1–2.5 μm . In the Top-Dep case, however, pH changes are more drastic across all size ranges: 0–1 μm (-0.17 units), 1–2.5 μm (-0.31 units), 2.5–5 μm (-0.35 units), and 5–10 μm (-0.33 units). These discrepancies between cases highlight that a reduction in NH_3 emissions enhances aerosol acidity (as in the Top-Dep case), but this effect can be partially offset by shifts in SO_4^{2-} and NO_3^- mass concentrations (as in the CEDS case). For instance, in the CEDS case, decreases in SO_4^{2-} and NO_3^- concentrations result in pH rises of 0.15–0.25 units across all size ranges compared to the Top-Dep case.

Our simulation results align with other studies. For example, Song et al. (2019) found that a ~ 0.3 increase in $\log_{10}[\text{NH}_3]$ contributed to a 0.3–0.4 unit rise in PM_{10} pH in Beijing during winter between 2014/2015 and 2018/2019. Concurrent changes in aerosol composition (increased NO_3^- and reduced SO_4^{2-} and Cl^-) led to a modest 0.1 units pH increase. Similarly, Zhou et al. (2022) observed a minor $\text{PM}_{2.5}$ pH decrease of -0.24 units in the Yangtze River Delta region from 2011 to 2019, despite significant changes in aerosol composition resulting from the Air Pollution Prevention and Control Action Plan.

7.2.2 Drivers of pH Changes

We further quantify the changes in pH values between the CEDS/Top-Dep cases and the base case, isolating the contributions from changes in H^+ and H_2O concentrations (detailed in Section 2.2.2). The results are presented in Figures S46S15 and S47S16.

In the CEDS case, the decreased pH values across all four aerosol size ranges are primarily driven by changes in H^+ concentrations, particularly over the remote regions of the Northern Hemisphere. The effects of H_2O concentration changes are particularly relevant in the Middle East and South Asia. Notably, a substantial pH increase is observed in South Asia, with increases of 0.35, 0.43, 0.44, and 0.63 units in the 0–1 μm , 1–2.5 μm , 2.5–5 μm , and 5–10 μm size ranges, respectively. These increases are predominantly caused by changes in H^+ concentrations, which fully counteract the pH-decreasing effects of changes in H_2O concentrations.

In the Top-Dep case, although changes in H^+ concentrations significantly enhance pH values in the 0–1 μm size range, the pH-decreasing effects of changes in H_2O concentrations are distributed across all four size ranges over the entire land surface. In East Asia, both H^+ and H_2O concentration changes contribute substantially to the observed pH decreases, highlighting their combined impact.

In summary, NH_3 emissions play a crucial role in maintaining terrestrial aerosols at moderately acidic levels,

particularly in the fine-mode size range of 0–1 μm . When NH_3/NH_3 emissions are completely removed in the model, the largest pH decreases are found in this size range. Our findings underscore that, in the fine-mode ranges (0–1 μm and 1–2.5 μm), pH changes closely correspond to variations in NH_3 emissions, reflecting the distinct sensitivity of size-resolved pH to NH_3 levels. In the coarser size ranges (2.5–5 μm and 5–10 μm), pH changes demonstrate a consistent trend with variations in NH_3 emissions in the fine-mode ranges (0–1 μm and 1–2.5 μm) based on our findings. Overall, pH changes in the fine-mode aerosols (0–1 μm and 1–2.5 μm) show a consistent response to variations in NH_3 emissions. However, increases in SO_4^{2-} and NO_3^- associated with elevated NH_3 emissions can partially offset the expected rise in pH (e.g., over land areas in the 1–2.5 μm range in the CEDS case). Furthermore, in regions with high SO_2 and NO_x emissions, such as East Asia under the CEDS inventory, the enhanced formation of SO_4^{2-} and NO_3^- can counteract the pH-lowering effect of reduced NH_3 emissions. In the coarser size ranges (2.5–5 μm and 5–10 μm), however, pH changes are governed by the competing influences of H^+ and H_2O concentration changes.

8. Conclusion

This study applied three distinct ammonia (NH_3)/ NH_3 emission schemes to the global atmospheric chemistry and climate model (EMAC) to assess the impact of NH_3/NH_3 emissions on the size-resolved sulfate-nitrate-ammonium (SNA) aerosol composition and aerosol acidity. It also explores the synergistic effects arising from concurrent changes in NH_3 , SO_2 , and NO_x emissions. The emission schemes included include two bottom-up inventories, and one inventory updated through a top-down approach. By simulating the aerosol size ranges of 0–1 μm , 1–2.5 μm , 2.5–5 μm , and 5–10 μm , the study provides a comprehensive analysis/assessment of the role of NH_3 how NH_3 emissions influence/influence global aerosol composition/chemistry and acidity across different particle size fractions.

The model accurately captures the distribution of global NH_3 hotspots, but comparisons with observational datasets reveal positive biases in NH_3/NH_3 concentrations and underestimations of $\text{NH}_4^+/\text{NH}_4^+$ in some regions such as China, North America, and Europe. This discrepancy suggests inefficiencies or oversimplifications in the $\text{NH}_3/\text{NH}_3/\text{NH}_3/\text{NH}_4^+$ partitioning treatment, with insufficient $\text{NH}_4^+/\text{NH}_4^+$ generated despite NH_3/NH_3 availability. In East and Southeast Asia, $\text{NH}_4^+/\text{NH}_4^+$ concentrations are well-simulated, but significant discrepancies were found for $\text{NO}_3^-/\text{NO}_3^-$ and $\text{SO}_4^{2-}/\text{SO}_4^{2-}$, likely due to the absence of heterogeneous oxidation processes in the model. The simulated global NH_3 burden and lifetime are higher than reported in related studies, attributed to the wet deposition scheme used in EMAC, which accounts for pH adjustments for NH_3 dissolution.

Over oceans, NH_3/NH_3 is entirely converted to $\text{NH}_4^+/\text{NH}_4^+$, while $\text{SO}_4^{2-}/\text{SO}_4^{2-}$ remains partially neutralized due to low NH_3/NH_3 emissions and high $\text{SO}_4^{2-}/\text{SO}_4^{2-}$ levels from biogenic dimethyl sulfide (DMS) emissions and $\text{NO}_3^-/\text{NO}_3^-$ and SO_2/SO_2 from shipping. Marine $\text{SO}_4^{2-}/\text{SO}_4^{2-}$ and $\text{NO}_3^-/\text{NO}_3^-$ are dominant in the super-micron modes, with mass fractions of 70% and 58%, respectively. Over land, SO_4^{2-} is total ammonia (the sum of NH_3 and NH_4^+) generally fully neutralized by NH_3 , exceeds SO_4^{2-} , enabling more complete neutralization, except in regions such as northern Russia, central Africa, and the Arabian Peninsula. Terrestrial $\text{NO}_3^-/\text{NO}_3^-$ is also largely neutralized by NH_3/NH_3 , resulting in over 60% of SNA concentrated in the sub-micron mode. In polluted areas such as East and South Asia,

sub-micron SNA fractions exceed 70%, with South Asia exhibiting nearly 90% sub-micron $\text{NH}_4^+/\text{NH}_4^+$. In contrast, the Middle East, dominated by dust and with minor NH_3 emissions, shows incomplete neutralization of $\text{SO}_4^{2-}/\text{SO}_4^{2-}$ and $\text{NO}_3^-/\text{NO}_3^-$. Here, nearly 70% of $\text{NO}_3^-/\text{NO}_3^-$ resides in the super-micron modes, while $\text{NH}_4^+/\text{NH}_4^+$ and $\text{SO}_4^{2-}/\text{SO}_4^{2-}$ dominate the sub-micron mode with respective mass fractions of 96% and 79%.

In the Northern Hemisphere, terrestrial aerosols are generally more acidic than marine aerosols, except in desert regions. Remote marine and desert aerosols remain neutral due to the alkaline influence of sea salt and non-volatile cations in dust, which enhance water uptake and neutralize $\text{SO}_4^{2-}/\text{SO}_4^{2-}$ and $\text{NO}_3^-/\text{NO}_3^-$. However, at high latitudes, marine aerosols become more acidic due to the long-range transport of anthropogenic pollutants from continental sources. The 0–1 μm size range exhibits higher pH values than the 1–2.5 μm range in many regions, a trend influenced by several factors. These include the assumption of a thermodynamically stable aerosol phase in the ISORROPIA model, the high sensitivity of aerosol acidity to NH_3 in the 0–1 μm range and observed lower concentrations of acidic components ($\text{SO}_4^{2-}/\text{SO}_4^{2-}$ and $\text{NO}_3^-/\text{NO}_3^-$) in this size range compared to larger sizes.

An 18% increase in NH_3 emissions over land leads to a significant increase in SNA concentrations in the 1–2.5 μm size range ($\text{NH}_4^+/\text{NH}_4^+$: 104%, $\text{NO}_3^-/\text{NO}_3^-$: 41%, $\text{SO}_4^{2-}/\text{SO}_4^{2-}$: 23%), while coarse mode SNA (2.5–10 μm) decreases. However, changes in size-resolved pH remain minimal, with the largest increase of 0.24 pH units occurring in the 0–1 μm range. In regions with low SNA, such as South America and Greenland, increased NH_3 emissions only lead to higher NH_3/NH_3 concentrations due to the limited availability of $\text{HNO}_3/\text{HNO}_3$ and $\text{H}_2\text{SO}_4/\text{H}_2\text{SO}_4$ for SNA formation. Conversely, in NH_3/NH_3 -rich regions such as East Asia and Europe, reductions in NH_3 emissions trigger compensatory effects, as excess NH_3/NH_3 and available SO_2/SO_2 and NO_x/NO_x help to maintain SNA formation despite the reduced NH_3/NH_3 supply. This highlights the buffering effect capacity of NH_3 plays a crucial role in stabilizing aerosol acidity in densely populated areas, mitigating the effects of fluctuations in regions. However, it is important to note that this buffering effect may be partially offset by concurrent increases in precursor gases, SO_2^{2-} and NO_3^- concentrations.

In summary, this study underscores the critical influence of NH_3/NH_3 emissions on global aerosol composition and acidity, with pronounced impacts on the size-resolved composition and properties of SNA aerosols. NH_3/NH_3 emissions significantly modulate aerosol acidity, particularly in sub-micron ranges, highlighting the sensitivity of fine-mode aerosols to NH_3/NH_3 levels. By buffering changes in aerosol pH, NH_3 emissions contribute to maintaining a relatively stable aerosol acidity, especially in heavily densely populated and heavily industrialized regions. These findings emphasize the importance of accurately representing NH_3/NH_3 dynamics in models for predicting atmospheric chemistry and climate interactions.

Code and Data Availability

1235 The usage of MESSy (Modular Earth Submodel System) and access to the source code is licensed to all affiliates of
institutions which are members of the MESSy Consortium. Institutions can become a member of the MESSy
Consortium by signing the “MESSy Memorandum of Understanding”. More information can be found on the MESSy
Consortium website: <http://www.messy-interface.org> (last access: 31 January 2025).
The code used in this study has been based on MESSy version 2.55 and is archived with a restricted access DOI
1240 (<https://doi.org/10.5281/zenodo.8379120>). The MESSy Consortium, (2023).
The data produced in the study is available from the authors upon request.

Acknowledgements

The work described in this paper has received funding from the Initiative and Networking Fund of the Helmholtz
Association through the project “Advanced Earth System Modelling Capacity (ESM)”. The authors gratefully
1245 acknowledge the Earth System Modelling Project (ESM) for funding this work by providing computing time on the
ESM partition of the supercomputer JUWELS (Alvarez, 2021) at the Jülich Supercomputing Centre (JSC). Xurong
Wang has been supported by the China Scholarship Council (CSC).

Competing Interests

At least one of the (co-)authors is a member of the editorial board of Atmospheric Chemistry and Physics.

1250 Author Contributions

XW and VAK planned the research and wrote the manuscript. XW performed the simulations and analyzed the results,
assisted by VAK and APT. XW and APT collected the observational data and conducted the model evaluation. XW
and ZL designed the Top-Dep case. All the authors discussed the results and contributed to the paper.

Reference

- 1255 Aas, W., Mortier, A., Bowersox, V., Cherian, R., Faluvegi, G., Fagerli, H., Hand, J., Klimont, Z., Galy-Lacaux, C.,
Lehmann, C. M. B., Myhre, C. L., Myhre, G., Olivie, D., Sato, K., Quaas, J., Rao, P. S. P., Schulz, M., Shindell,
D., Skeie, R. B., Stein, A., Takemura, T., Tsyro, S., Vet, R., and Xu, X.: Global and regional trends of atmospheric
sulfur, Scientific Reports, 9, 953, 10.1038/s41598-018-37304-0, 2019.
- Alexander, L., Allen, S., Bindoff, N., Breon, F.-M., Church, J., Cubasch, U., Emori, S., Forster, P., Friedlingstein, P.,
1260 Gillett, N., Gregory, J., Hartmann, D., Jansen, E., Kirtman, B., Knutti, R., Kanikicharla, K., Lemke, P., Marotzke,
J., Masson-Delmotte, V., and Xie, S.-P.: Climate change 2013: The physical science basis, in contribution of
Working Group I (WGI) to the Fifth Assessment Report (AR5) of the Intergovernmental Panel on Climate Change
(IPCC), in, 2013.
- 1265 Allen, H. M., Draper, D. C., Ayres, B. R., Ault, A., Bondy, A., Takahama, S., Modini, R. L., Baumann, K., Edgerton,
E., Knote, C., Laskin, A., Wang, B., and Fry, J. L.: Influence of crustal dust and sea spray supermicron particle
concentrations and acidity on inorganic NO_3^- aerosol during the 2013 Southern
Oxidant and Aerosol Study, Atmos. Chem. Phys., 15, 10669-10685, 10.5194/acp-15-10669-2015, 2015.
- Andreae, M., Berresheim, H., Bingemer, H., Jacob, D. J., Lewis, B., Li, S. M., and Talbot, R. W.: The atmospheric
sulfur cycle over the Amazon Basin: 2. Wet season, Journal of Geophysical Research: Atmospheres, 95, 16813-
1270 16824, 1990.
- Andreae, M. O.: Aerosols Before Pollution, Science, 315, 50-51, doi:10.1126/science.1136529, 2007.
- Andreae, M. O.: Emission of trace gases and aerosols from biomass burning – an updated assessment, Atmos. Chem.
Phys., 19, 8523-8546, 10.5194/acp-19-8523-2019, 2019.
- Astitha, M., Lelieveld, J., Abdel Kader, M., Pozzer, A., and de Meij, A.: Parameterization of dust emissions in the

Formatted: Indent: Hanging: 0.51 cm

1275 global atmospheric chemistry-climate model EMAC: impact of nudging and soil properties, *Atmos. Chem. Phys.*,
12, 11057-11083, 10.5194/acp-12-11057-2012, 2012.

| Bacer, S., Sullivan, S. C., Karydis, V. A., Barahona, D., Krämer, M., Nenes, A., Tost, H., Tsimpidi, A. P., Lelieveld, J.,
and Pozzer, A.: Implementation of a comprehensive ice crystal formation parameterization for cirrus and mixed-
1280 phase clouds in the EMAC model (based on MESSy 2.53), *Geosci. Model Dev.*, 11, 4021-4041, 10.5194/gmd-11-
4021-2018, 2018.

Beusen, A. H. W., Bouwman, A. F., Heuberger, P. S. C., Van Drecht, G., and Van Der Hoek, K. W.: Bottom-up
uncertainty estimates of global ammonia emissions from global agricultural production systems, *Atmospheric*
Environment, 42, 6067-6077, <https://doi.org/10.1016/j.atmosenv.2008.03.044>, 2008.

1285 Bian, H., Chin, M., Hauglustaine, D. A., Schulz, M., Myhre, G., Bauer, S. E., Lund, M. T., Karydis, V. A., Kucsera, T.
L., Pan, X., Pozzer, A., Skeie, R. B., Steenrod, S. D., Sudo, K., Tsigaridis, K., Tsimpidi, A. P., and Tsyro, S. G.:
Investigation of global particulate nitrate from the AeroCom phase III experiment, *Atmos. Chem. Phys.*, 17, 12911-
12940, 10.5194/acp-17-12911-2017, 2017.

Bleeker, A., Vries, W. d., Dentener, F., Sutton, M. A., Reis, S., Riddick, S. N., Dragosits, U., Nemitz, E., Theobald, M.
R., Tang, Y. S., Braban, C. F., Veno, M., Dore, A. J., Mitchell, R. F., Wanless, S., Daunt, F., Fowler, D., Blackall,
1290 T. D., Milford, C., Flechard, C. R., Loubet, B., Massad, R., Cellier, P., Coheur, P. F., Clarisse, L., Damme, M. v.,
Ngadi, Y., Clerbaux, C., Ambelas Skjoth, C., Geels, C., Hertel, O., Wichink Kruit, R. J., Pinder, R. W., Bash, J. O.,
Walker, J. D., Simpson, D., Horvath, L., and Misselbrook, T. H.: Towards a climate-dependent paradigm of
ammonia emission and deposition, urn:NBN:nl:ui:24-uuid:1516f098-ca7e-402b-a05d-83633f8c2612, 2013.

1295 Bougiatioti, A., Nikolaou, P., Stavroulas, I., Kouvarakis, G., Weber, R., Nenes, A., Kanakidou, M., and Mihalopoulos,
N.: Particle water and pH in the eastern Mediterranean: source variability and implications for nutrient availability,
Atmos. Chem. Phys., 16, 4579-4591, 10.5194/acp-16-4579-2016, 2016.

Bouwman, A. F., Boumans, L. J. M., and Batjes, N. H.: Estimation of global NH₃ volatilization loss from synthetic
fertilizers and animal manure applied to arable lands and grasslands, *Global Biogeochemical Cycles*, 16, 8-1-8-
14, <https://doi.org/10.1029/2000GB001389>, 2002.

1300 Bouwman, A. F., Lee, D. S., Asman, W. A. H., Dentener, F. J., Van Der Hoek, K. W., and Olivier, J. G. J.: A global
high-resolution emission inventory for ammonia, *Global Biogeochemical Cycles*, 11, 561-587,
<https://doi.org/10.1029/97GB02266>, 1997.

Burgard, D. A. and Briä, C. R. M.: Bridge-based sensing of NO_x and SO₂ emissions from ocean-going ships,
Atmospheric Environment, 136, 54-60, <https://doi.org/10.1016/j.atmosenv.2016.04.014>, 2016.

1305 Cai, S., Wang, Y., Zhao, B., Wang, S., Chang, X., and Hao, J.: The impact of the "Air Pollution Prevention and Control
Action Plan" on PM_{2.5} concentrations in Jing-Jin-Ji region during 2012–2020, *Science of The Total Environment*,
580, 197-209, <https://doi.org/10.1016/j.scitotenv.2016.11.188>, 2017.

Cavalli, F., Facchini, M. C., Decesari, S., Mircea, M., Emblico, L., Fuzzi, S., Ceburnis, D., Yoon, Y. J., O'Dowd, C.
D., Putaud, J.-P., and Dell'Acqua, A.: Advances in characterization of size-resolved organic matter in marine
1310 aerosol over the North Atlantic, *Journal of Geophysical Research: Atmospheres*, 109,
<https://doi.org/10.1029/2004JD005137>, 2004.

Chang, Y., Zou, Z., Zhang, Y., Deng, C., Hu, J., Shi, Z., Dore, A. J., and Collett, J. L., Jr.: Assessing Contributions of
Agricultural and Nonagricultural Emissions to Atmospheric Ammonia in a Chinese Megacity, *Environmental*
Science & Technology, 53, 1822-1833, 10.1021/acs.est.8b05984, 2019.

1315 Che, H., Zhang, X., Li, Y., Zhou, Z., Qu, J. J., and Hao, X.: Haze trends over the capital cities of 31 provinces in
China, 1981–2005, *Theoretical and Applied Climatology*, 97, 235-242, 10.1007/s00704-008-0059-8, 2009.

Chen, D., Liu, Z., Fast, J., and Ban, J.: Simulations of sulfate–nitrate–ammonium (SNA) aerosols during the extreme
haze events over northern China in October 2014, *Atmos. Chem. Phys.*, 16, 10707-10724, 10.5194/acp-16-10707-
2016, 2016.

1320 Chen, Y., Shen, H., and Russell, A. G.: Current and Future Responses of Aerosol pH and Composition in the U.S. to
Declining SO₂ Emissions and Increasing NH₃ Emissions, *Environmental Science & Technology*, 53, 9646-9655,
10.1021/acs.est.9b02005, 2019.

Chen, Y., Cheng, Y., Ma, N., Wei, C., Ran, L., Wolke, R., Größ, J., Wang, Q., Pozzer, A., Denier van der Gon, H. A.
C., Spindler, G., Lelieveld, J., Tegen, I., Su, H., and Wiedensohler, A.: Natural sea-salt emissions moderate the
1325 climate forcing of anthropogenic nitrate, *Atmos. Chem. Phys.*, 20, 771-786, 10.5194/acp-20-771-2020, 2020.

Chen, Y., Shen, H., Kaiser, J., Hu, Y., Capps, S. L., Zhao, S., Hakami, A., Shih, J. S., Pavur, G. K., Turner, M. D.,
Henze, D. K., Resler, J., Nenes, A., Napelenok, S. L., Bash, J. O., Fahey, K. M., Carmichael, G. R., Chai, T.,
Clarisse, L., Coheur, P. F., Van Damme, M., and Russell, A. G.: High-resolution hybrid inversion of IASI ammonia
columns to constrain US ammonia emissions using the CMAQ adjoint model, *Atmos. Chem. Phys.*, 21, 2067-
1330 2082, 10.5194/acp-21-2067-2021, 2021.

- Cheng, Y., Zheng, G., Wei, C., Mu, Q., Zheng, B., Wang, Z., Gao, M., Zhang, Q., He, K., Carmichael, G., Pöschl, U., and Su, H.: Reactive nitrogen chemistry in aerosol water as a source of sulfate during haze events in China, *Science Advances*, 2, e1601530, doi:10.1126/sciadv.1601530, 2016.
- 1335 Clarisse, L., Clerbaux, C., Dentener, F., Hurtmans, D., and Coheur, P.-F.: Global ammonia distribution derived from infrared satellite observations, *Nature Geoscience*, 2, 479-483, 10.1038/ngeo551, 2009.
- Colette, A., Granier, C., Hodnebrog, Ø., Jakobs, H., Maurizi, A., Nyiri, A., Bessagnet, B., D'Angiola, A., D'Isidoro, M., Gauss, M., Meleux, F., Memmesheimer, M., Mieville, A., Rouil, L., Russo, F., Solberg, S., Stordal, F., and Tampieri, F.: Air quality trends in Europe over the past decade: a first multi-model assessment, *Atmos. Chem. Phys.*, 11, 11657-11678, 10.5194/acp-11-11657-2011, 2011.
- 1340 Craig, R. L., Peterson, P. K., Nandy, L., Lei, Z., Hossain, M. A., Camarena, S., Dodson, R. A., Cook, R. D., Dutcher, C. S., and Ault, A. P.: Direct Determination of Aerosol pH: Size-Resolved Measurements of Submicrometer and Supermicrometer Aqueous Particles, *Analytical Chemistry*, 90, 11232-11239, 10.1021/acs.analchem.8b00586, 2018.
- 1345 Crippa, M., Guizzardi, D., Muntean, M., Schaaf, E., Dentener, F., van Aardenne, J. A., Monni, S., Doering, U., Olivier, J. G. J., Pagliari, V., and Janssens-Maenhout, G.: Gridded emissions of air pollutants for the period 1970–2012 within EDGAR v4.3.2, *Earth Syst. Sci. Data*, 10, 1987-2013, 10.5194/essd-10-1987-2018, 2018.
- Dammers, E., McLinden, C. A., Griffin, D., Shephard, M. W., Van Der Graaf, S., Lutsch, E., Schaap, M., Gainairu-Matz, Y., Fioletov, V., Van Damme, M., Whitburn, S., Clarisse, L., Cady-Pereira, K., Clerbaux, C., Coheur, P. F., and Erisman, J. W.: NH₃ emissions from large point sources derived from CrIS and IASI satellite observations, *Atmos. Chem. Phys.*, 19, 12261-12293, 10.5194/acp-19-12261-2019, 2019.
- 1350 Dammers, E., Shephard, M. W., Palm, M., Cady-Pereira, K., Capps, S., Lutsch, E., Strong, K., Hannigan, J. W., Ortega, I., Toon, G. C., Stremme, W., Grutter, M., Jones, N., Smale, D., Siemons, J., Hrpcek, K., Tremblay, D., Schaap, M., Notholt, J., and Erisman, J. W.: Validation of the CrIS fast physical NH₃ retrieval with ground-based FTIR, *Atmos. Meas. Tech.*, 10, 2645-2667, 10.5194/amt-10-2645-2017, 2017.
- 1355 Delon, C., Galy-Lacaux, C., Adon, M., Liousse, C., Serça, D., Diop, B., and Akpo, A.: Nitrogen compounds emission and deposition in West African ecosystems: comparison between wet and dry savanna, *Biogeosciences*, 9, 385-402, 10.5194/bg-9-385-2012, 2012.
- Dentener, F. J. and Crutzen, P. J.: A three-dimensional model of the global ammonia cycle, *Journal of Atmospheric Chemistry*, 19, 331-369, 10.1007/BF00694492, 1994.
- 1360 Ding, J., Zhao, P., Su, J., Dong, Q., Du, X., and Zhang, Y.: Aerosol pH and its driving factors in Beijing, *Atmos. Chem. Phys.*, 19, 7939-7954, 10.5194/acp-19-7939-2019, 2019.
- Dockery, D. W., Pope, C. A., Xu, X., Spengler, J. D., Ware, J. H., Fay, M. E., Ferris, B. G., and Speizer, F. E.: An Association between Air Pollution and Mortality in Six U.S. Cities, *New England Journal of Medicine*, 329, 1753-1759, 10.1056/nejm199312093292401, 1993.
- 1365 Dockery, D. W., Cunningham, J., Damokosh, A. I., Neas, L. M., Spengler, J. D., Koutrakis, P., Ware, J. H., Raizenne, M., and Speizer, F. E.: Health effects of acid aerosols on North American children: respiratory symptoms, *Environmental Health Perspectives*, 104, 500-505, doi:10.1289/ehp.96104500, 1996.
- Erisman, J. W. and Schaap, M.: The need for ammonia abatement with respect to secondary PM reductions in Europe, *Environ Pollut*, 129, 159-163, 10.1016/j.envpol.2003.08.042, 2004.
- 1370 Fang, T., Guo, H., Zeng, L., Verma, V., Nenes, A., and Weber, R. J.: Highly Acidic Ambient Particles, Soluble Metals, and Oxidative Potential: A Link between Sulfate and Aerosol Toxicity, *Environmental Science & Technology*, 51, 2611-2620, 10.1021/acs.est.6b06151, 2017.
- Fiddes, S. L., Woodhouse, M. T., Nicholls, Z., Lane, T. P., and Schofield, R.: Cloud, precipitation and radiation responses to large perturbations in global dimethyl sulfide, *Atmos. Chem. Phys.*, 18, 10177-10198, 10.5194/acp-18-10177-2018, 2018.
- 1375 Fortems-Cheiney, A., Dufour, G., Foret, G., Siour, G., Van Damme, M., Coheur, P.-F., Clarisse, L., Clerbaux, C., and Beekmann, M.: Understanding the Simulated Ammonia Increasing Trend from 2008 to 2015 over Europe with CHIMERE and Comparison with IASI Observations, *Atmosphere*, 13, 1101, 2022.
- Fountoukis, C. and Nenes, A.: ISORROPIA II: a computationally efficient thermodynamic equilibrium model for K^{+} – Ca^{2+} – Mg^{2+} – NH_4^{+} – Na^{+} – SO_4^{2-} – NO_3^{-} – Cl^{-} – H_2O aerosols, *Atmos. Chem. Phys.*, 7, 4639-4659, 10.5194/acp-7-4639-2007, 2007.
- 1380 Fu, X., Wang, S., Xing, J., Zhang, X., Wang, T., and Hao, J.: Increasing Ammonia Concentrations Reduce the Effectiveness of Particle Pollution Control Achieved via SO₂ and NO_x Emissions Reduction in East China, *Environmental Science & Technology Letters*, 4, 221-227, 10.1021/acs.estlett.7b00143, 2017.
- 1385

- Ge, Y., Vieno, M., Stevenson, D. S., Wind, P., and Heal, M. R.: A new assessment of global and regional budgets, fluxes, and lifetimes of atmospheric reactive N and S gases and aerosols, *Atmos. Chem. Phys.*, 22, 8343–8368, 10.5194/acp-22-8343-2022, 2022.
- 1390 Gong, C., Tian, H., Liao, H., Pan, N., Pan, S., Ito, A., Jain, A. K., Kou-Giesbrecht, S., Joos, F., Sun, Q., Shi, H., Vuichard, N., Zhu, Q., Peng, C., Maggi, F., Tang, F. H. M., and Zechle, S.: Global net climate effects of anthropogenic reactive nitrogen, *Nature*, 632, 557–563, 10.1038/s41586-024-07714-4, 2024.
- 1395 Gu, B., Zhang, L., Van Dingenen, R., Vieno, M., Van Grinsven, H. J., Zhang, X., Zhang, S., Chen, Y., Wang, S., Ren, C., Rao, S., Holland, M., Winiwarter, W., Chen, D., Xu, J., and Sutton, M. A.: Abating ammonia is more cost-effective than nitrogen oxides for mitigating PM_{2.5} air pollution, *Science*, 374, 758–762, doi:10.1126/science.abf8623, 2021.
- Guo, H., Weber, R. J., and Nenes, A.: High levels of ammonia do not raise fine particle pH sufficiently to yield nitrogen oxide-dominated sulfate production, *Scientific Reports*, 7, 12109, 10.1038/s41598-017-11704-0, 2017a.
- 1400 Guo, H., Otjes, R., Schlag, P., Kiendler-Scharr, A., Nenes, A., and Weber, R. J.: Effectiveness of ammonia reduction on control of fine particle nitrate, *Atmos. Chem. Phys.*, 18, 12241–12256, 10.5194/acp-18-12241-2018, 2018.
- Guo, H., Liu, J., Froyd, K. D., Roberts, J. M., Veres, P. R., Hayes, P. L., Jimenez, J. L., Nenes, A., and Weber, R. J.: Fine particle pH and gas–particle phase partitioning of inorganic species in Pasadena, California, during the 2010 CalNex campaign, *Atmos. Chem. Phys.*, 17, 5703–5719, 10.5194/acp-17-5703-2017, 2017b.
- 1405 Guo, H., Sullivan, A. P., Campuzano-Jost, P., Schroder, J. C., Lopez-Hilfiker, F. D., Dibb, J. E., Jimenez, J. L., Thornton, J. A., Brown, S. S., Nenes, A., and Weber, R. J.: Fine particle pH and the partitioning of nitric acid during winter in the northeastern United States, *Journal of Geophysical Research: Atmospheres*, 121, 10,355–310,376, <https://doi.org/10.1002/2016JD025311>, 2016.
- Guo, H., Xu, L., Bougiatioti, A., Cerully, K. M., Capps, S. L., Hite Jr, J. R., Carlton, A. G., Lee, S. H., Bergin, M. H., Ng, N. L., Nenes, A., and Weber, R. J.: Fine-particle water and pH in the southeastern United States, *Atmos. Chem. Phys.*, 15, 5211–5228, 10.5194/acp-15-5211-2015, 2015.
- 1410 Hand, J. L., Schichtel, B. A., Malm, W. C., and Pitchford, M. L.: Particulate sulfate ion concentration and SO₂ emission trends in the United States from the early 1990s through 2010, *Atmos. Chem. Phys.*, 12, 10353–10365, 10.5194/acp-12-10353-2012, 2012.
- 1415 Hauglustaine, D. A., Balkanski, Y., and Schulz, M.: A global model simulation of present and future nitrate aerosols and their direct radiative forcing of climate, *Atmos. Chem. Phys.*, 14, 11031–11063, 10.5194/acp-14-11031-2014, 2014.
- Heald, C. L., Collett Jr, J. L., Lee, T., Benedict, K. B., Schwandner, F. M., Li, Y., Clarisse, L., Hurtmans, D. R., Van Damme, M., Clerbaux, C., Coheur, P. F., Philip, S., Martin, R. V., and Pye, H. O. T.: Atmospheric ammonia and particulate inorganic nitrogen over the United States, *Atmos. Chem. Phys.*, 12, 10295–10312, 10.5194/acp-12-10295-2012, 2012.
- 1420 Hersbach, H., Bell, B., Berrisford, P., Hirahara, S., Horányi, A., Muñoz-Sabater, J., Nicolas, J., Peubey, C., Radu, R., Schepers, D., Simmons, A., Soci, C., Abdalla, S., Abellan, X., Balsamo, G., Bechtold, P., Biavati, G., Bidlot, J., Bonavita, M., De Chiara, G., Dahlgren, P., Dee, D., Diamantakis, M., Dragani, R., Flemming, J., Forbes, R., Fuentes, M., Geer, A., Haimberger, L., Healy, S., Hogan, R. J., Hólm, E., Janisková, M., Keeley, S., Laloyaux, P., Lopez, P., Lupu, C., Radnoti, G., de Rosnay, P., Rozum, I., Vamborg, F., Villaume, S., and Thépaut, J.-N.: The ERA5 global reanalysis, *Quarterly Journal of the Royal Meteorological Society*, 146, 1999–2049, <https://doi.org/10.1002/qj.3803>, 2020.
- 1425 Hickman, J. E., Andela, N., Tsigaridis, K., Galy-Lacaux, C., Ossohou, M., Dammers, E., Van Damme, M., Clarisse, L., and Bauer, S. E.: Continental and Ecoregion-Specific Drivers of Atmospheric NO₂ and NH₃ Seasonality Over Africa Revealed by Satellite Observations, *Global Biogeochemical Cycles*, 35, e2020GB006916, <https://doi.org/10.1029/2020GB006916>, 2021.
- 1430 Hoesly, R. M., Smith, S. J., Feng, L., Klimont, Z., Janssens-Maenhout, G., Pitkanen, T., Seibert, J. J., Vu, L., Andres, R. J., Bolt, R. M., Bond, T. C., Dawidowski, L., Kholod, N., Kurokawa, J. I., Li, M., Liu, L., Lu, Z., Moura, M. C. P., O'Rourke, P. R., and Zhang, Q.: Historical (1750–2014) anthropogenic emissions of reactive gases and aerosols from the Community Emissions Data System (CEDS), *Geosci. Model Dev.*, 11, 369–408, 10.5194/gmd-11-369-2018, 2018.
- 1435 Huang, X., Zhang, J., Zhang, W., Tang, G., and Wang, Y.: Atmospheric ammonia and its effect on PM_{2.5} pollution in urban Chengdu, Sichuan Basin, China, *Environmental Pollution*, 291, 118195, <https://doi.org/10.1016/j.envpol.2021.118195>, 2021.
- 1440 Intergovernmental Panel on Climate, C. (Ed.): Climate Change 2022 - Mitigation of Climate Change: Working Group III Contribution to the Sixth Assessment Report of the Intergovernmental Panel on Climate Change, Cambridge University Press, Cambridge, DOI: 10.1017/9781009157926, 2023.

1445

1450

1455

1460

1465

1470

1475

1480

1485

1490

1495

IPCC: Climate Change 2013: The Physical Science Basis. Contribution of Working Group I to the Fifth Assessment Report of the Intergovernmental Panel on Climate Change, Cambridge, United Kingdom and New York, NY, USA, 1535, 2013.

[IPCC, 2022: Climate Change 2022: Mitigation of Climate Change. Contribution of Working Group III to the Sixth Assessment Report of the Intergovernmental Panel on Climate Change \[P.R. Shukla, J. Skea, R. Slade, A. Al Khouridajie, R. van Diemen, D. McCollum, M. Pathak, S. Some, P. Vyas, R. Fradera, M. Belkacemi, A. Hasija, G. Lisboa, S. Luz, J. Malley. \(eds.\)\]. Cambridge University Press, Cambridge, UK and New York, NY, USA. doi: 10.1017/9781009157926](#)

Jackson, R. L., Gabric, A. J., Cropp, R., and Woodhouse, M. T.: Dimethylsulfide (DMS), marine biogenic aerosols and the ecophysiology of coral reefs, *Biogeosciences*, 17, 2181-2204, 10.5194/bg-17-2181-2020, 2020.

Jo, Y.-J., Lee, H.-J., Jo, H.-Y., Woo, J.-H., Kim, Y., Lee, T., Heo, G., Park, S.-M., Jung, D., Park, J., and Kim, C.-H.: Changes in inorganic aerosol compositions over the Yellow Sea area from impact of Chinese emissions mitigation, *Atmospheric Research*, 240, 104948, <https://doi.org/10.1016/j.atmosres.2020.104948>, 2020.

Jöckel, P., Sander, R., Kerkweg, A., Tost, H., and Lelieveld, J.: Technical Note: The Modular Earth Submodel System (MESSy) - a new approach towards Earth System Modeling, *Atmos. Chem. Phys.*, 5, 433-444, 10.5194/acp-5-433-2005, 2005.

Jöckel, P., Kerkweg, A., Pozzer, A., Sander, R., Tost, H., Riede, H., Baumgaertner, A., Gromov, S., and Kern, B.: Development cycle 2 of the Modular Earth Submodel System (MESSy2), *Geosci. Model Dev.*, 3, 717-752, 10.5194/gmd-3-717-2010, 2010.

Jöckel, P., Tost, H., Pozzer, A., Kunze, M., Kirner, O., Brenninkmeijer, C., Brinkop, S., Cai, D. S., Dyroff, C., and Eckstein, J.: Earth System Chemistry Integrated Modelling (ESCiMo) with the Modular Earth Submodel System (MESSy, version 2.51), *Geoscientific Model Development*, 9, 1153-1200, 2016.

Kaiser, J. W., Heil, A., Andreae, M. O., Benedetti, A., Chubarova, N., Jones, L., Morcrette, J. J., Razinger, M., Schultz, M. G., Suttie, M., and van der Werf, G. R.: Biomass burning emissions estimated with a global fire assimilation system based on observed fire radiative power, *Biogeosciences*, 9, 527-554, 10.5194/bg-9-527-2012, 2012.

Kakavas, S., Patoulas, D., Zakoura, M., Nenes, A., and Pandis, S. N.: Size-resolved aerosol pH over Europe during summer, *Atmos. Chem. Phys.*, 21, 799-811, 10.5194/acp-21-799-2021, 2021.

Karydis, V. A., Tsimpidi, A. P., Pozzer, A., and Lelieveld, J.: How alkaline compounds control atmospheric aerosol particle acidity, *Atmos. Chem. Phys.*, 21, 14983-15001, 10.5194/acp-21-14983-2021, 2021.

Karydis, V. A., Tsimpidi, A. P., Lei, W., Molina, L. T., and Pandis, S. N.: Formation of semivolatile inorganic aerosols in the Mexico City Metropolitan Area during the MILAGRO campaign, *Atmos. Chem. Phys.*, 11, 13305-13323, 10.5194/acp-11-13305-2011, 2011.

Karydis, V. A., Tsimpidi, A. P., Pozzer, A., Astitha, M., and Lelieveld, J.: Effects of mineral dust on global atmospheric nitrate concentrations, *Atmos. Chem. Phys.*, 16, 1491-1509, 10.5194/acp-16-1491-2016, 2016.

Karydis, V. A., Tsimpidi, A. P., Bacer, S., Pozzer, A., Nenes, A., and Lelieveld, J.: Global impact of mineral dust on cloud droplet number concentration, *Atmos. Chem. Phys.*, 17, 5601-5621, 10.5194/acp-17-5601-2017, 2017.

Karydis, V. A., Tsimpidi, A. P., Fountoukis, C., Nenes, A., Zavala, M., Lei, W., Molina, L. T., and Pandis, S. N.: Simulating the fine and coarse inorganic particulate matter concentrations in a polluted megacity, *Atmospheric Environment*, 44, 608-620, <https://doi.org/10.1016/j.atmosenv.2009.11.023>, 2010.

Kerkweg, A., Buchholz, J., Ganzeveld, L., Pozzer, A., Tost, H., and Jöckel, P.: Technical Note: An implementation of the dry removal processes DRY DEposition and SEDimentation in the Modular Earth Submodel System (MESSy), *Atmos. Chem. Phys.*, 6, 4617-4632, 10.5194/acp-6-4617-2006, 2006.

Khan, M. A. H., Lowe, D., Derwent, R. G., Foulds, A., Chhantyal-Pun, R., McFiggans, G., Orr-Ewing, A. J., Percival, C. J., and Shallcross, D. E.: Global and regional model simulations of atmospheric ammonia, *Atmospheric Research*, 234, 104702, <https://doi.org/10.1016/j.atmosres.2019.104702>, 2020.

Klingmüller, K., Metzger, S., Abdelkader, M., Karydis, V. A., Stenchikov, G. L., Pozzer, A., and Lelieveld, J.: Revised mineral dust emissions in the atmospheric chemistry-climate model EMAC (MESSy 2.52 DU_Astitha1 KKDU2017 patch), *Geosci. Model Dev.*, 11, 989-1008, 10.5194/gmd-11-989-2018, 2018.

Koçak, M., Mihalopoulos, N., and Kubilay, N.: Chemical composition of the fine and coarse fraction of aerosols in the northeastern Mediterranean, *Atmospheric Environment*, 41, 7351-7368, <https://doi.org/10.1016/j.atmosenv.2007.05.011>, 2007.

Kong, L., Tang, X., Zhu, J., Wang, Z., Pan, Y., Wu, H., Wu, L., Wu, Q., He, Y., Tian, S., Xie, Y., Liu, Z., Sui, W., Han, L., and Carmichael, G.: Improved Inversion of Monthly Ammonia Emissions in China Based on the Chinese Ammonia Monitoring Network and Ensemble Kalman Filter, *Environmental Science & Technology*, 53, 12529-12538, 10.1021/acs.est.9b02701, 2019.

Lei, L., Zhou, W., Chen, C., He, Y., Li, Z., Sun, J., Tang, X., Fu, P., Wang, Z., and Sun, Y.: Long-term characterization

- of aerosol chemistry in cold season from 2013 to 2020 in Beijing, China, *Environmental Pollution*, 268, 115952, <https://doi.org/10.1016/j.envpol.2020.115952>, 2021.
- 1500 Li, C., Martin, R. V., van Donkelaar, A., Boys, B. L., Hammer, M. S., Xu, J.-W., Marais, E. A., Reff, A., Strum, M., Ridley, D. A., Crippa, M., Brauer, M., and Zhang, Q.: Trends in Chemical Composition of Global and Regional Population-Weighted Fine Particulate Matter Estimated for 25 Years, *Environmental Science & Technology*, 51, 11185-11195, [10.1021/acs.est.7b02530](https://doi.org/10.1021/acs.est.7b02530), 2017.
- 1505 Li, K., Chen, L., White, S. J., Yu, H., Wu, X., Gao, X., Azzi, M., and Cen, K.: Smog chamber study of the role of NH₃ in new particle formation from photo-oxidation of aromatic hydrocarbons, *Science of The Total Environment*, 619-620, 927-937, <https://doi.org/10.1016/j.scitotenv.2017.11.180>, 2018.
- 1510 Liu, J., Ding, P., Zong, Z., Li, J., Tian, C., Chen, W., Chang, M., Salazar, G., Shen, C., Cheng, Z., Chen, Y., Wang, X., Szidat, S., and Zhang, G.: Evidence of Rural and Suburban Sources of Urban Haze Formation in China: A Case Study From the Pearl River Delta Region, *Journal of Geophysical Research: Atmospheres*, 123, 4712-4726, <https://doi.org/10.1029/2017JD027952>, 2018a.
- Liu, L., Xu, W., Lu, X., Zhong, B., Guo, Y., Lu, X., Zhao, Y., He, W., Wang, S., Zhang, X., Liu, X., and Vitousek, P.: Exploring global changes in agricultural ammonia emissions and their contribution to nitrogen deposition since 1980, *Proceedings of the National Academy of Sciences*, 119, e2121998119, [doi:10.1073/pnas.2121998119](https://doi.org/10.1073/pnas.2121998119), 2022.
- 1515 Liu, M., Song, Y., Zhou, T., Xu, Z., Yan, C., Zheng, M., Wu, Z., Hu, M., Wu, Y., and Zhu, T.: Fine particle pH during severe haze episodes in northern China, *Geophysical Research Letters*, 44, 5213-5221, <https://doi.org/10.1002/2017GL073210>, 2017.
- Liu, M., Huang, X., Song, Y., Xu, T., Wang, S., Wu, Z., Hu, M., Zhang, L., Zhang, Q., Pan, Y., Liu, X., and Zhu, T.: Rapid SO₂ emission reductions significantly increase tropospheric ammonia concentrations over the North China Plain, *Atmos. Chem. Phys.*, 18, 17933-17943, [10.5194/acp-18-17933-2018](https://doi.org/10.5194/acp-18-17933-2018), 2018b.
- 1520 Lohmann, U. and Ferrachat, S.: Impact of parametric uncertainties on the present-day climate and on the anthropogenic aerosol effect, *Atmos. Chem. Phys.*, 10, 11373-11383, [10.5194/acp-10-11373-2010](https://doi.org/10.5194/acp-10-11373-2010), 2010.
- Luo, Z., Zhang, Y., Chen, W., Van Damme, M., Coheur, P. F., and Clarisse, L.: Estimating global ammonia (NH₃) emissions based on IASI observations from 2008 to 2018, *Atmos. Chem. Phys.*, 22, 10375-10388, [10.5194/acp-22-10375-2022](https://doi.org/10.5194/acp-22-10375-2022), 2022.
- 1525 McDuffie, E. E., Smith, S. J., O'Rourke, P., Tibrewal, K., Venkataraman, C., Marais, E. A., Zheng, B., Crippa, M., Brauer, M., and Martin, R. V.: A global anthropogenic emission inventory of atmospheric pollutants from sector- and fuel-specific sources (1970–2017): an application of the Community Emissions Data System (CEDS), *Earth Syst. Sci. Data*, 12, 3413-3442, [10.5194/essd-12-3413-2020](https://doi.org/10.5194/essd-12-3413-2020), 2020.
- 1530 Milousis, A., Tsimpidi, A. P., Tost, H., Pandis, S. N., Nenes, A., Kiendler-Scharr, A., and Karydis, V. A.: Implementation of the ISORROPIA-lite aerosol thermodynamics model into the EMAC chemistry climate model (based on MESSy v2.55): implications for aerosol composition and acidity, *Geosci. Model Dev.*, 17, 1111-1131, [10.5194/gmd-17-1111-2024](https://doi.org/10.5194/gmd-17-1111-2024), 2024.
- [Milousis, A., Scholz, S. M. C., Fuchs, H., Tsimpidi, A. P., and Karydis, V. A.: Global Perspectives on Nitrate Aerosol Dynamics: A Comprehensive Sensitivity Analysis, *EGUsphere*, 2025, 1-42, 10.5194/egusphere-2025-313](https://doi.org/10.5194/egusphere-2025-313), 2025.
- 1535 Morán, M., Ferreira, J., Martins, H., Monteiro, A., Borrego, C., and González, J. A.: Ammonia agriculture emissions: From EMEP to a high resolution inventory, *Atmospheric Pollution Research*, 7, 786-798, <https://doi.org/10.1016/j.apr.2016.04.001>, 2016.
- [Myhre, G., Samset, B. H., Schulz, M., Balkanski, Y., Bauer, S., Bernsten, T. K., Bian, H., Bellouin, N., Chin, M., Diehl, T., Easter, R. C., Feichter, J., Ghan, S. J., Hauglustaine, D., Iversen, T., Kinne, S., Kirkevåg, A., Lamarque, J. F., Lin, G., Liu, X., Lund, M. T., Luo, G., Ma, X., van Noije, T., Penner, J. E., Rasch, P. J., Ruiz, A., Seland, Ø., Skeie, R. B., Stier, P., Takemura, T., Tsigaridis, K., Wang, P., Wang, Z., Xu, L., Yu, H., Yu, F., Yoon, J. H., Zhang, K., Zhang, H., and Zhou, C.: Radiative forcing of the direct aerosol effect from AeroCom Phase II simulations, *Atmos. Chem. Phys.*, 13, 1853-1877, 10.5194/acp-13-1853-2013](https://doi.org/10.5194/acp-13-1853-2013), 2013.
- 1540 Nenes, A., Pandis, S. N., and Pilinis, C.: ISORROPIA: A New Thermodynamic Equilibrium Model for Multiphase Multicomponent Inorganic Aerosols, *Aquatic Geochemistry*, 4, 123-152, [10.1023/A:1009604003981](https://doi.org/10.1023/A:1009604003981), 1998.
- 1545 Nenes, A., Pandis, S. N., Weber, R. J., and Russell, A.: Aerosol pH and liquid water content determine when particulate matter is sensitive to ammonia and nitrate availability, *Atmos. Chem. Phys.*, 20, 3249-3258, [10.5194/acp-20-3249-2020](https://doi.org/10.5194/acp-20-3249-2020), 2020.
- 1550 Olivier, J. G. J., Bouwman, A. F., Van der Hoek, K. W., and Berdowski, J. J. M.: Global air emission inventories for anthropogenic sources of NO_x, NH₃ and N₂O in 1990, *Environmental Pollution*, 102, 135-148, [https://doi.org/10.1016/S0269-7491\(98\)80026-2](https://doi.org/10.1016/S0269-7491(98)80026-2), 1998.
- Osipov, S., Chowdhury, S., Crowley, J. N., Tadic, I., Drewnick, F., Borrmann, S., Eger, P., Fachinger, F., Fischer, H., Predybaylo, E., Fnais, M., Harder, H., Pikridas, M., Vouterakos, P., Pozzer, A., Sciare, J., Ukhov, A., Stenchikov,

1555 G. L., Williams, J., and Lelieveld, J.: Severe atmospheric pollution in the Middle East is attributable to anthropogenic sources, *Communications Earth & Environment*, 3, 203, 10.1038/s43247-022-00514-6, 2022.

Pan, Y., Tian, S., Liu, D., Fang, Y., Zhu, X., Zhang, Q., Zheng, B., Michalski, G., and Wang, Y.: Fossil Fuel Combustion-Related Emissions Dominate Atmospheric Ammonia Sources during Severe Haze Episodes: Evidence from (15)N-Stable Isotope in Size-Resolved Aerosol Ammonium, *Environ Sci Technol*, 50, 8049-8056, 10.1021/acs.est.6b00634, 2016.

1560 Pozzer, A., Reifenberg, S. F., Kumar, V., Franco, B., Kohl, M., Taraborrelli, D., Gromov, S., Ehrhart, S., Jöckel, P., Sander, R., Fall, V., Rosanka, S., Karydis, V., Akritidis, D., Emmerichs, T., Crippa, M., Guizzardi, D., Kaiser, J. W., Clarisse, L., Kiendler-Scharr, A., Tost, H., and Tsimpidi, A.: Simulation of organics in the atmosphere: evaluation of EMACv2.54 with the Mainz Organic Mechanism (MOM) coupled to the ORACLE (v1.0) submodel, *Geosci. Model Dev.*, 15, 2673-2710, 10.5194/gmd-15-2673-2022, 2022.

1565 Pozzer, A., Tsimpidi, A. P., Karydis, V. A., de Meij, A., and Lelieveld, J.: Impact of agricultural emission reductions on fine-particulate matter and public health, *Atmos. Chem. Phys.*, 17, 12813-12826, 10.5194/acp-17-12813-2017, 2017.

Pringle, K. J., Tost, H., Message, S., Steil, B., Giannadaki, D., Nenes, A., Fountoukis, C., Stier, P., Vignati, E., and Lelieveld, J.: Description and evaluation of GMX: a new aerosol submodel for global simulations (v1), *Geosci. Model Dev.*, 3, 391-412, 10.5194/gmd-3-391-2010, 2010.

1570 Prospero, J. M., Savoie, D. L., Nees, R. T., Duce, R. A., and Merrill, J.: Particulate sulfate and nitrate in the boundary layer over the North Pacific Ocean, *Journal of Geophysical Research: Atmospheres*, 90, 10586-10596, <https://doi.org/10.1029/JD090iD06p10586>, 1985.

1575 Pye, H. O. T., Nenes, A., Alexander, B., Ault, A. P., Barth, M. C., Clegg, S. L., Collett Jr, J. L., Fahey, K. M., Hennigan, C. J., Herrmann, H., Kanakidou, M., Kelly, J. T., Ku, I. T., McNeill, V. F., Riemer, N., Schaefer, T., Shi, G., Tilgner, A., Walker, J. T., Wang, T., Weber, R., Xing, J., Zaveri, R. A., and Zuend, A.: The acidity of atmospheric particles and clouds, *Atmos. Chem. Phys.*, 20, 4809-4888, 10.5194/acp-20-4809-2020, 2020.

1580 Roeckner, E., Brokopf, R., Esch, M., Giorgetta, M., Hagemann, S., Kornbluh, L., Manzini, E., Schlese, U., and Schulzweida, U.: Sensitivity of simulated climate to horizontal and vertical resolution in the ECHAM5 atmosphere model, *Journal of Climate*, 19, 3771-3791, 10.1175/jcli3824.1, 2006.

Russell, A. R., Valin, L. C., and Cohen, R. C.: Trends in OMI NO₂ observations over the United States: effects of emission control technology and the economic recession, *Atmos. Chem. Phys.*, 12, 12197-12209, 10.5194/acp-12-12197-2012, 2012.

1585 Russell, L. M., Moore, R. H., Burrows, S. M., and Quinn, P. K.: Ocean flux of salt, sulfate, and organic components to atmospheric aerosol, *Earth-Science Reviews*, 239, 104364, <https://doi.org/10.1016/j.earscirev.2023.104364>, 2023.

Sahoo, P., Sahu, S. K., Mangaraj, P., Mishra, A., Beig, G., and Gunthe, S. S.: Reporting of gridded ammonia emission and assessment of hotspots across India: A comprehensive study of 24 anthropogenic sources, *Journal of Hazardous Materials*, 479, 135557, <https://doi.org/10.1016/j.jhazmat.2024.135557>, 2024.

1590 Sander, R., Baumgaertner, A., Cabrera-Perez, D., Frank, F., Gromov, S., Groß, J. U., Harder, H., Huijnen, V., Jöckel, P., Karydis, V. A., Niemeyer, K. E., Pozzer, A., Riede, H., Schultz, M. G., Taraborrelli, D., and Tauer, S.: The community atmospheric chemistry box model CAABA/MECCA-4.0, *Geosci. Model Dev.*, 12, 1365-1385, 10.5194/gmd-12-1365-2019, 2019.

1595 Schlesinger, W. H. and Hartley, A. E.: A global budget for atmospheric NH₃, *Biogeochemistry*, 15, 191-211, 10.1007/BF00002936, 1992.

Seinfeld, J. H. and Pandis, S. N.: *Atmospheric chemistry and physics : from air pollution to climate change*, Third edition, John Wiley & Sons, Inc. Hoboken, New Jersey, Hoboken, New Jersey 2016.

1600 Shah, V., Jaeglé, L., Thornton, J. A., Lopez-Hilfiker, F. D., Lee, B. H., Schroder, J. C., Campuzano-Jost, P., Jimenez, J. L., Guo, H., Sullivan, A. P., Weber, R. J., Green, J. R., Fiddler, M. N., Bililign, S., Campos, T. L., Stell, M., Weinheimer, A. J., Montzka, D. D., and Brown, S. S.: Chemical feedbacks weaken the wintertime response of particulate sulfate and nitrate to emissions reductions over the eastern United States, *Proceedings of the National Academy of Sciences*, 115, 8110-8115, doi:10.1073/pnas.1803295115, 2018.

1605 Shi, G., Xu, J., Peng, X., Xiao, Z., Chen, K., Tian, Y., Guan, X., Feng, Y., Yu, H., Nenes, A., and Russell, A. G.: pH of Aerosols in a Polluted Atmosphere: Source Contributions to Highly Acidic Aerosol, *Environmental Science & Technology*, 51, 4289-4296, 10.1021/acs.est.6b05736, 2017.

Shi, G., Xu, J., Shi, X., Liu, B., Bi, X., Xiao, Z., Chen, K., Wen, J., Dong, S., Tian, Y., Feng, Y., Yu, H., Song, S., Zhao, Q., Gao, J., and Russell, A. G.: Aerosol pH Dynamics During Haze Periods in an Urban Environment in China: Use of Detailed, Hourly, Speciated Observations to Study the Role of Ammonia Availability and Secondary Aerosol Formation and Urban Environment, *Journal of Geophysical Research: Atmospheres*, 124, 9730-9742,

1610

- <https://doi.org/10.1029/2018JD029976>, 2019.
- Skjoth, C. A. and Geels, C.: The effect of climate and climate change on ammonia emissions in Europe, *Atmos. Chem. Phys.*, 13, 117-128, 10.5194/acp-13-117-2013, 2013.
- Sogaard, H. T., Sommer, S. G., Hutchings, N. J., Huijsmans, J. F. M., Bussink, D. W., and Nicholson, F.: Ammonia volatilization from field-applied animal slurry—the ALFAM model, *Atmospheric Environment*, 36, 3309-3319, [https://doi.org/10.1016/S1352-2310\(02\)00300-X](https://doi.org/10.1016/S1352-2310(02)00300-X), 2002.
- Song, S., Nenes, A., Gao, M., Zhang, Y., Liu, P., Shao, J., Ye, D., Xu, W., Lei, L., Sun, Y., Liu, B., Wang, S., and McElroy, M. B.: Thermodynamic Modeling Suggests Declines in Water Uptake and Acidity of Inorganic Aerosols in Beijing Winter Haze Events during 2014/2015–2018/2019, *Environmental Science & Technology Letters*, 6, 752-760, 10.1021/acs.estlett.9b00621, 2019.
- Spengler, J. D., Koutrakis, P., Dockery, D. W., Raizenne, M., and Speizer, F. E.: Health effects of acid aerosols on North American children: air pollution exposures, *Environmental Health Perspectives*, 104, 492-499, doi:10.1289/ehp.96104492, 1996.
- Thurston, G. D., Ito, K., Hayes, C. G., Bates, D. V., and Lippmann, M.: Respiratory Hospital Admissions and Summertime Haze Air Pollution in Toronto, Ontario: Consideration of the Role of Acid Aerosols, *Environmental Research*, 65, 271-290, <https://doi.org/10.1006/enrs.1994.1037>, 1994.
- Tilgner, A., Schaefer, T., Alexander, B., Barth, M., Collett Jr, J. L., Fahey, K. M., Nenes, A., Pye, H. O. T., Herrmann, H., and McNeill, V. F.: Acidity and the multiphase chemistry of atmospheric aqueous particles and clouds, *Atmos. Chem. Phys.*, 21, 13483-13536, 10.5194/acp-21-13483-2021, 2021.
- Tost, H., Jöckel, P., Kerkweg, A., Sander, R., and Lelieveld, J.: Technical note: A new comprehensive SCAVenging submodel for global atmospheric chemistry modelling, *Atmos. Chem. Phys.*, 6, 565-574, 10.5194/acp-6-565-2006, 2006.
- Tsimpidi, A. P., Karydis, V. A., and Pandis, S. N.: Response of Inorganic Fine Particulate Matter to Emission Changes of Sulfur Dioxide and Ammonia: The Eastern United States as a Case Study, *Journal of the Air & Waste Management Association*, 57, 1489-1498, 10.3155/1047-3289.57.12.1489, 2007.
- Tsimpidi, A. P., Karydis, V. A., Pozzer, A., Pandis, S. N., and Lelieveld, J.: [Global combustion sources of ORACLE \(v1.0\): module to simulate the organic aerosols: model comparison with 84 AMS factor analysis data sets, Atmos. aerosol composition and evolution in the atmosphere, Geosci. Model Dev., 7, 3153-3172](#), *Atmos. Chem. Phys.*, 16, 8939-8962, 10.5194/acp-16-8939-2016, 2016, [gmd-7-3153-2014, 2014](#).
- Tsimpidi, A. P., Karydis, V. A., Pandis, S. N., and Lelieveld, J.: [Global-scale combustion sources of organic aerosols: sensitivity to formation and removal mechanisms, Atmospheric Chemistry and Physics, 17, 7345-7364, 10.5194/acp-17-7345-2017, 2017](#).
- Tsimpidi, A. P., Karydis, V. A., Pozzer, A., Pandis, S. N., and Lelieveld, J.: [ORACLE \(v2.0\): an efficient module to simulate the volatility and oxygen content of organic aerosol composition and evolution in the atmosphere, Geosci. Model Dev., 7, 3153-3172](#), *Development*, 11, 3369-3389, 10.5194/gmd-7-3153-2014, 2014, [11-3369-2018, 2018](#).
- Tsimpidi, A. P., Scholz, S. M. C., Milousis, A., Mihalopoulos, N., and Karydis, V. A.: [Aerosol Composition Trends during 2000-2020: In depth insights from model predictions and multiple worldwide observation datasets, EGUSphere, 2024, 1-66, 10.5194/egusphere-2024-3590, 2024](#).
- van Aardenne, J. A., Dentener, F. J., Olivier, J. G. J., Goldewijk, C. G. M. K., and Lelieveld, J.: A 1°×1° resolution data set of historical anthropogenic trace gas emissions for the period 1890–1990, *Global Biogeochemical Cycles*, 15, 909-928, <https://doi.org/10.1029/2000GB001265>, 2001.
- Van Damme, M., Clarisse, L., Whitburn, S., Hadji-Lazaro, J., Hurtmans, D., Clerbaux, C., and Coheur, P.-F.: Industrial and agricultural ammonia point sources exposed, *Nature*, 564, 99-103, 10.1038/s41586-018-0747-1, 2018.
- Van Damme, M., Erisman, J. W., Clarisse, L., Dammers, E., Whitburn, S., Clerbaux, C., Dolman, A. J., and Coheur, P.-F.: Worldwide spatiotemporal atmospheric ammonia (NH₃) columns variability revealed by satellite, *Geophysical Research Letters*, 42, 8660-8668, <https://doi.org/10.1002/2015GL065496>, 2015.
- Van Damme, M., Clarisse, L., Heald, C. L., Hurtmans, D., Ngadi, Y., Clerbaux, C., Dolman, A. J., Erisman, J. W., and Coheur, P. F.: Global distributions, time series and error characterization of atmospheric ammonia (NH₃) from IASI satellite observations, *Atmos. Chem. Phys.*, 14, 2905-2922, 10.5194/acp-14-2905-2014, 2014.
- Vasilakos, P., Russell, A., Weber, R., and Nenes, A.: [Understanding nitrate formation in a world with less sulfate, Atmos. Chem. Phys., 18, 12765-12775, 10.5194/acp-18-12765-2018, 2018](#).
- Vignati, E., Wilson, J., and Stier, P.: M7: An efficient size-resolved aerosol microphysics module for large-scale aerosol transport models, *Journal of Geophysical Research*, 109, 10.1029/2003JD004485, 2004.
- Walker, J. M., Philip, S., Martin, R. V., and Seinfeld, J. H.: Simulation of nitrate, sulfate, and ammonium aerosols over

Formatted: Indent: Hanging: 0.51 cm

Formatted: Indent: Hanging: 0.51 cm

the United States, *Atmos. Chem. Phys.*, 12, 11213-11227, 10.5194/acp-12-11213-2012, 2012.

1670 Wang, G., Zhang, R., Gomez, M. E., Yang, L., Levy Zamora, M., Hu, M., Lin, Y., Peng, J., Guo, S., Meng, J., Li, J., Cheng, C., Hu, T., Ren, Y., Wang, Y., Gao, J., Cao, J., An, Z., Zhou, W., Li, G., Wang, J., Tian, P., Marrero-Ortiz, W., Secrest, J., Du, Z., Zheng, J., Shang, D., Zeng, L., Shao, M., Wang, W., Huang, Y., Wang, Y., Zhu, Y., Li, Y., Hu, J., Pan, B., Cai, L., Cheng, Y., Ji, Y., Zhang, F., Rosenfeld, D., Liss, P. S., Duce, R. A., Kolb, C. E., and Molina, M. J.: Persistent sulfate formation from London Fog to Chinese haze, *Proceedings of the National Academy of Sciences*, 113, 13630-13635, doi:10.1073/pnas.1616540113, 2016.

1675 Wang, M., Kong, W., Marten, R., He, X.-C., Chen, D., Pfeifer, J., Heitto, A., Kontkanen, J., Dada, L., Kürten, A., Yli-Juuti, T., Manninen, H. E., Amanatidis, S., Amorim, A., Baalbaki, R., Baccarini, A., Bell, D. M., Bertozzi, B., Bräkling, S., Brilke, S., Murillo, L. C., Chiu, R., Chu, B., De Menezes, L.-P., Duplissy, J., Finkenzeller, H., Carracedo, L. G., Granzin, M., Guida, R., Hansel, A., Hofbauer, V., Krechmer, J., Lehtipalo, K., Lamkaddam, H., Lampimäki, M., Lee, C. P., Makhmutov, V., Marie, G., Mathot, S., Mauldin, R. L., Mentler, B., Müller, T., Onnela, A., Partoll, E., Petäjä, T., Philippov, M., Pospisilova, V., Ranjithkumar, A., Rissanen, M., Rörup, B., Scholz, W., Shen, J., Simon, M., Sipilä, M., Steiner, G., Stolzenburg, D., Tham, Y. J., Tomé, A., Wagner, A. C., Wang, D. S., Wang, Y., Weber, S. K., Winkler, P. M., Wlasits, P. J., Wu, Y., Xiao, M., Ye, Q., Zauner-Wieczorek, M., Zhou, X., Volkamer, R., Riipinen, I., Dommen, J., Curtius, J., Baltensperger, U., Kulmala, M., Worsnop, D. R., Kirkby, J., Seinfeld, J. H., El-Haddad, I., Flagan, R. C., and Donahue, N. M.: Rapid growth of new atmospheric particles by nitric acid and ammonia condensation, *Nature*, 581, 184-189, 10.1038/s41586-020-2270-4, 2020.

1680 Wang, S., Xing, J., Jang, C., Zhu, Y., Fu, J. S., and Hao, J.: Impact Assessment of Ammonia Emissions on Inorganic Aerosols in East China Using Response Surface Modeling Technique, *Environmental Science & Technology*, 45, 9293-9300, 10.1021/es2022347, 2011.

1685 Wang, X., Zhang, C., Gao, Y., Ji, X., Su, W., and Liu, C.: Satellite unravels recent changes in atmospheric nitrogen oxides emissions from global ocean shipping, *Journal of Cleaner Production*, 429, 139591, <https://doi.org/10.1016/j.jclepro.2023.139591>, 2023.

1690 Wang, X., Wang, W., Yang, L., Gao, X., Nie, W., Yu, Y., Xu, P., Zhou, Y., and Wang, Z.: The secondary formation of inorganic aerosols in the droplet mode through heterogeneous aqueous reactions under haze conditions, *Atmospheric Environment*, 63, 68-76, <https://doi.org/10.1016/j.atmosenv.2012.09.029>, 2012.

1695 Wang, Y., Zhang, Q. Q., He, K., Zhang, Q., and Chai, L.: Sulfate-nitrate-ammonium aerosols over China: response to 2000–2015 emission changes of sulfur dioxide, nitrogen oxides, and ammonia, *Atmos. Chem. Phys.*, 13, 2635-2652, 10.5194/acp-13-2635-2013, 2013.

Warner, J. X., Dickerson, R. R., Wei, Z., Strow, L. L., Wang, Y., and Liang, Q.: Increased atmospheric ammonia over the world's major agricultural areas detected from space, *Geophysical Research Letters*, 44, 2875-2884, <https://doi.org/10.1002/2016GL072305>, 2017.

1700 Weber, R. J., Guo, H., Russell, A. G., and Nenes, A.: High aerosol acidity despite declining atmospheric sulfate concentrations over the past 15 years, *Nature Geoscience*, 9, 282-285, 10.1038/ngeo2665, 2016.

West, J. J., Ansari, A. S., and Pandis, S. N.: Marginal PM_{2.5}: Nonlinear Aerosol Mass Response to Sulfate Reductions in the Eastern United States, *Journal of the Air & Waste Management Association*, 49, 1415-1424, 10.1080/10473289.1999.10463973, 1999.

1705 Xie, X., Hu, J., Qin, M., Guo, S., Hu, M., Wang, H., Lou, S., Li, J., Sun, J., Li, X., Sheng, L., Zhu, J., Chen, G., Yin, J., Fu, W., Huang, C., and Zhang, Y.: Modeling particulate nitrate in China: Current findings and future directions, *Environment International*, 166, 107369, <https://doi.org/10.1016/j.envint.2022.107369>, 2022.

Xu, J., Chen, J., Zhao, N., Wang, G., Yu, G., Li, H., Huo, J., Lin, Y., Fu, Q., Guo, H., Deng, C., Lee, S. H., Chen, J., and Huang, K.: Importance of gas-particle partitioning of ammonia in haze formation in the rural agricultural environment, *Atmos. Chem. Phys.*, 20, 7259-7269, 10.5194/acp-20-7259-2020, 2020.

1710 Xu, P., Li, G., Zheng, Y., Fung, J. C. H., Chen, A., Zeng, Z., Shen, H., Hu, M., Mao, J., Zheng, Y., Cui, X., Guo, Z., Chen, Y., Feng, L., He, S., Zhang, X., Lau, A. K. H., Tao, S., and Houlton, B. Z.: Fertilizer management for global ammonia emission reduction, *Nature*, 626, 792-798, 10.1038/s41586-024-07020-z, 2024.

1715 Xu, P., Liao, Y. J., Lin, Y. H., Zhao, C. X., Yan, C. H., Cao, M. N., Wang, G. S., and Luan, S. J.: High-resolution inventory of ammonia emissions from agricultural fertilizer in China from 1978 to 2008, *Atmos. Chem. Phys.*, 16, 1207-1218, 10.5194/acp-16-1207-2016, 2016.

Xu, R., Tian, H., Pan, S., Prior, S. A., Feng, Y., Batchelor, W. D., Chen, J., and Yang, J.: Global ammonia emissions from synthetic nitrogen fertilizer applications in agricultural systems: Empirical and process-based estimates and uncertainty, *Global Change Biology*, 25, 314-326, <https://doi.org/10.1111/gcb.14499>, 2019.

1720 Yao, W., Zhang, C., Hao, H., Wang, X., and Li, X.: A support vector machine approach to estimate global solar radiation with the influence of fog and haze, *Renewable Energy*, 128, 155-162, <https://doi.org/10.1016/j.renene.2018.05.069>, 2018.

- Yu, F., Nair, A. A., and Luo, G.: Long-Term Trend of Gaseous Ammonia Over the United States: Modeling and Comparison With Observations, *Journal of Geophysical Research: Atmospheres*, 123, 8315-8325, <https://doi.org/10.1029/2018JD028412>, 2018.
- 1725 Zhang, B., Shen, H., Liu, P., Guo, H., Hu, Y., Chen, Y., Xie, S., Xi, Z., Skipper, T. N., and Russell, A. G.: Significant contrasts in aerosol acidity between China and the United States, *Atmos. Chem. Phys.*, 21, 8341-8356, 10.5194/acp-21-8341-2021, 2021a.
- 1730 Zhang, L., Chen, Y., Zhao, Y., Henze, D. K., Zhu, L., Song, Y., Paulot, F., Liu, X., Pan, Y., Lin, Y., and Huang, B.: Agricultural ammonia emissions in China: reconciling bottom-up and top-down estimates, *Atmos. Chem. Phys.*, 18, 339-355, 10.5194/acp-18-339-2018, 2018.
- 1735 Zhang, L., Gong, S., Zhao, T., Zhou, C., Wang, Y., Li, J., Ji, D., He, J., Liu, H., Gui, K., Guo, X., Gao, J., Shan, Y., Wang, H., Wang, Y., Che, H., and Zhang, X.: Development of WRF/CUACE v1.0 model and its preliminary application in simulating air quality in China, *Geosci. Model Dev.*, 14, 703-718, 10.5194/gmd-14-703-2021, 2021b.
- Zhang, Q. and Geng, G.: Impact of clean air action on PM2.5 pollution in China, *Science China Earth Sciences*, 62, 1845-1846, 10.1007/s11430-019-9531-4, 2019.
- 1740 Zhao, P., Zhang, X., Xu, X., and Zhao, X.: Long-term visibility trends and characteristics in the region of Beijing, Tianjin, and Hebei, China, *Atmospheric Research*, 101, 711-718, <https://doi.org/10.1016/j.atmosres.2011.04.019>, 2011.
- Zheng, B., Zhang, Q., Zhang, Y., He, K. B., Wang, K., Zheng, G. J., Duan, F. K., Ma, Y. L., and Kimoto, T.: Heterogeneous chemistry: a mechanism missing in current models to explain secondary inorganic aerosol formation during the January 2013 haze episode in North China, *Atmos. Chem. Phys.*, 15, 2031-2049, 10.5194/acp-15-2031-2015, 2015.
- 1745 Zheng, B., Tong, D., Li, M., Liu, F., Hong, C., Geng, G., Li, H., Li, X., Peng, L., Qi, J., Yan, L., Zhang, Y., Zhao, H., Zheng, Y., He, K., and Zhang, Q.: Trends in China's anthropogenic emissions since 2010 as the consequence of clean air actions, *Atmos. Chem. Phys.*, 18, 14095-14111, 10.5194/acp-18-14095-2018, 2018.
- Zheng, G., Su, H., and Cheng, Y.: Revisiting the Key Driving Processes of the Decadal Trend of Aerosol Acidity in the U.S, *ACS Environmental Au*, 2, 346-353, 10.1021/acsenvironau.1c00055, 2022.
- 1750 Zheng, G., Su, H., Andreae, M. O., Pöschl, U., and Cheng, Y.: Multiphase Buffering by Ammonia Sustains Sulfate Production in Atmospheric Aerosols, *AGU Advances*, 5, e2024AV001238, <https://doi.org/10.1029/2024AV001238>, 2024.
- Zheng, G., Su, H., Wang, S., Andreae, M. O., Pöschl, U., and Cheng, Y.: Multiphase buffer theory explains contrasts in atmospheric aerosol acidity, *Science*, 369, 1374-1377, doi:10.1126/science.aba3719, 2020.
- 1755 Zhou, M., Deng, Z., Robert, C., Zhang, X., Zhang, L., Wang, Y., Qi, C., Wang, P., and Mazière, M. D.: The First Global Map of Atmospheric Ammonia (NH₃) as Observed by the HIRAS/FY-3D Satellite, *Advances in Atmospheric Sciences*, 41, 379-390, 10.1007/s00376-023-3059-9, 2024.
- Zhou, M., Zheng, G., Wang, H., Qiao, L., Zhu, S., Huang, D., An, J., Lou, S., Tao, S., Wang, Q., Yan, R., Ma, Y., Chen, C., Cheng, Y., Su, H., and Huang, C.: Long-term trends and drivers of aerosol pH in eastern China, *Atmos. Chem. Phys.*, 22, 13833-13844, 10.5194/acp-22-13833-2022, 2022.
- 1760 Zhou, W., Gao, M., He, Y., Wang, Q., Xie, C., Xu, W., Zhao, J., Du, W., Qiu, Y., Lei, L., Fu, P., Wang, Z., Worsnop, D. R., Zhang, Q., and Sun, Y.: Response of aerosol chemistry to clean air action in Beijing, China: Insights from two-year ACSM measurements and model simulations, *Environmental Pollution*, 255, 113345, <https://doi.org/10.1016/j.envpol.2019.113345>, 2019.